

RESEARCH ARTICLE

Extreme warm events in the South Orkney Islands, Southern Ocean: Compounding influence of atmospheric rivers and föhn conditions

Hua Lu  | Andrew Orr  | John King | Tony Phillips | Ella Gilbert |
Steve Colwell | Thomas J. Bracegirdle

British Antarctic Survey, Cambridge, UK

Correspondence

Hua Lu, British Antarctic Survey,
Cambridge, UK.

Email: hlu@bas.ac.uk

Funding information

British Antarctic Survey, Grant/Award
Number: NE/X009319/1; Horizon 2020
Framework Programme, Grant/Award
Number: 101003590; Natural
Environment Research Council

Abstract

Extreme warm events in the South Orkney Islands (SOIs) are investigated using synoptic observations from Signy and Orcadas stations for 1947–1994 and 1956–2019 respectively. Defining the extremes as temperatures exceeding the 95th percentile of the temperature distribution, we reveal the characteristics and associated drivers of the warm events, especially the top 10 events in both summer and winter. At both stations, extreme warm events often involve a combined effect of atmospheric rivers (ARs) and localised föhn warming, with distinct characteristics due to the station locations relative to Coronation Island, the largest and highest island of the SOIs. For example, warm events at Signy are warmer (by an average of around 3°C) than the corresponding concurrent temperatures at Orcadas. The number of warm events per year has significantly increased over the record periods at both stations, which could potentially impact ecosystems by increasing melting of snow and ice. Extreme warm events at Signy are dominated by föhn warming in combination with ARs originating from the Southern Atlantic Ocean, where warm, moisture-rich air is rapidly advected towards the islands by enhanced northerly winds. By contrast, the Orcadas warm extremes involve both warm-air advection and föhn warming associated with enhanced northwesterlies/westerlies with ARs originating in the Pacific Ocean that travel across the Drake Passage. Simulation of one of the top 10 warm events for Signy station using a 1-km grid spacing configuration of the atmosphere-only UK Met Office Unified Model is used to disentangle the role of local versus large-scale forcing. We find that the majority of the warming can be attributed to föhn effects for the case study. These results demonstrate the complexity of Antarctic temperature extremes.

KEYWORDS

atmospheric rivers, circulation-orography interactions, extreme temperature events, föhn warming, sub-Antarctic islands

1 | INTRODUCTION

Small, isolated, mountainous islands within the Antarctic polar front of the Southern Ocean, such as the South Orkney Islands (SOIs), South Georgia and the South Sandwich Islands, South Shetland Islands, and the Kerguelen Islands are important Antarctic terrestrial ecosystems and areas of biodiversity (Convey, 2017; Colesie *et al.*, 2023). Extreme warm air temperatures over these islands can result in ecosystem change either by exceeding upper tolerance thresholds or causing melting of snow and ice fields, for example, leading to the altered patterns of water availability and exposure of the underlying soil and vegetation (Smith, 1990; Calosi *et al.*, 2008; Convey, 2017; Colesie *et al.*, 2023). However, although a comprehensive investigation of extreme warm-temperature occurrences in these maritime islands is of fundamental concern, studies of this kind remain very scarce. For instance, extreme temperatures in the SOIs have been studied based on the observations from a single station as part of an Antarctica-wide investigation with little information regarding the within-SOIs variation (Turner *et al.*, 2021).

The mountainous SOIs archipelago is situated about 600 km from the Antarctic Peninsula, consisting of four main islands that are largely glaciated (Coronation Island, Laurie Island, Powell Island, and Signy Island) and numerous smaller islets (Figure 1). Coronation Island is the largest and highest island of the SOIs (46 km long, 5.6–14.8 km wide, and up to 1,265 m high) and is located immediately north of Signy Island and west of Laurie Island. Signy Island in particular is characterised by relatively extensive vegetation and wildlife populations as it is the least glaciated of the four main islands (Smith, 1990; Cannone *et al.*, 2017). These islands are also surrounded by waters that are part of the Weddell-Scotia confluence zone, which are some of the most dynamic and productive waters in the Southern Ocean (Sanchez *et al.*, 2019). This region is thus of great importance in terms of both Antarctic ecological systems and the global oceanic circulation (Meredith *et al.*, 2015; Convey, 2017).

Like most of the maritime and sub-Antarctic islands, the SOIs lie within the region of the prevailing westerly winds, and are thus subject to intense cyclonic and anti-cyclonic activities in association with the southern extratropical storm tracks (Hoskins and Hodges, 2005). These weather systems bring in moist air masses from the relatively warm South Pacific or Southern Atlantic Oceans to the SOIs, as well as cold air from the ice-covered Weddell Sea, resulting in large temperature variation as well as shaping both atmospheric and oceanographic conditions of the surrounding regions (Turner *et al.*, 2021). In addition, their interaction with the pronounced local orography and land–sea

contrast strongly influences temperature, precipitation, and winds, via topographically induced warming (föhn winds), rain shadowing, upstream flow deceleration, and acceleration at the corners of islands (Hunt *et al.*, 2004; Orr *et al.*, 2005; Risien and Chelton, 2008; Hosking *et al.*, 2014; King *et al.*, 2017; Bannister and King, 2020; Alves *et al.*, 2021; Turner *et al.*, 2021).

Because of the geographical setting of the SOIs, Coronation Island will likely produce significant localised föhn (leeside) warming to Signy Island in response to northerly or northwesterly winds, as suggested by King *et al.* (2017). Föhn events raise leeside temperatures through various mechanisms, including the leeside descent of potentially warmer air from aloft (so-called ‘isentropic drawdown’), latent heating associated with orographic precipitation over the windward slope, and sensible heating through turbulent mixing (Elvidge and Renfrew, 2016). Indeed, the extreme warm temperature of 19.8°C recorded on 30 January 1982 at Signy station (on Signy Island) was induced by a combination of large-scale advection of warm air from north of the SOIs and local amplification by two successive föhn events (King *et al.*, 2017). During this time the temperature recorded at Orcadas station, situated only 51 km away on Laurie Island (Figure 1), was 16.8°C lower and not notable as a warm event. Similarly, as Laurie Island is located downwind of Coronation Island with respect to the prevailing westerlies it is also possibly affected by föhn warming, which Turner *et al.* (2021) speculated was the cause of extreme warm temperatures at Orcadas station (on Laurie Island). Thus, these previous studies suggest that the occurrence of extreme warm events could be highly spatially variable across the SOIs. To date, however, there is only one case study investigating föhn warming over the SOIs, which focused on Signy Island (King *et al.*, 2017), and little is known about the spatial and seasonal variation of extreme temperature events in relation to the island’s complex orography.

Some of the extreme warm-temperature events that occur over the Antarctic are linked to atmospheric rivers (ARs) — long and narrow filament-shaped structures that carry abundant heat and moisture from the subtropics (Wille *et al.*, 2019). The large-scale circulation anomalies that bring ARs towards Antarctica are often associated with intense extratropical cyclones termed ‘atmospheric bombs’ and blocking high events (Wille *et al.*, 2019; Zhang *et al.*, 2019). Moreover, föhn events have been shown to enhance warming associated with ARs over the Antarctic Peninsula; their combined effect has been found to be responsible for record warm temperatures for continental Antarctica (Bozkurt *et al.*, 2018; Wille *et al.*, 2022). However, the large-scale circulation patterns that are responsible for warm-temperature extremes over the SOIs remain poorly understood, particularly the importance of

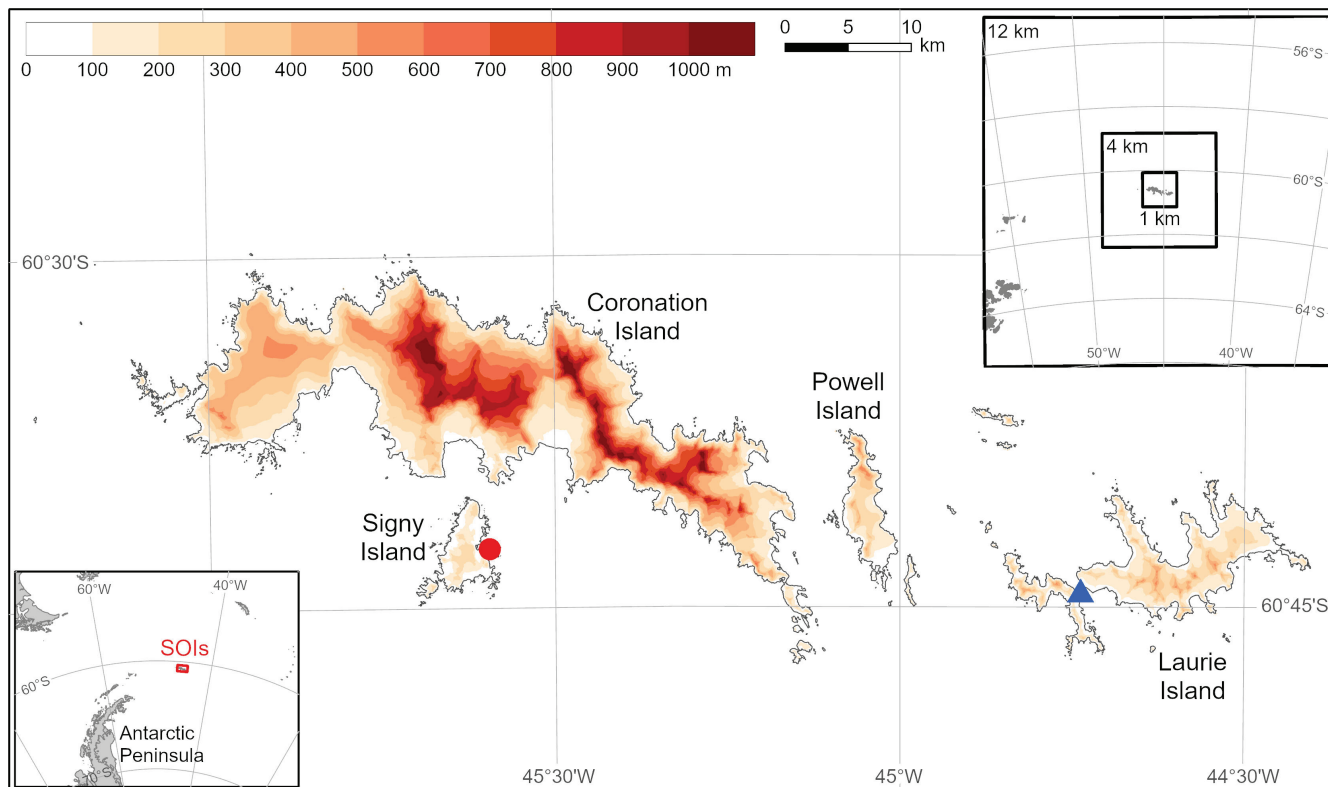


FIGURE 1 Map showing the location and height of orography (m) of the South Orkney Islands (SOIs), as well as the names of its four main islands and the locations of Signy and Orcadas research stations (indicated by a red circle and blue triangle respectively). The map in the bottom left-hand corner shows the location of the SOIs relative to the Antarctic Peninsula. The upper right-hand corner shows the MetUM model domains at grid spacings of 12, 4, and 1 km. The orography shown is generated from the 100-m-resolution version of the REMA v1.1 (Howat *et al.*, 2022).

ARs and their potential to generate föhn events to create additional warming.

Extreme warm-temperature events in the Antarctic region typically last for a few hours to a couple of days (Turner *et al.*, 2021; Maclennan *et al.*, 2022; Wille *et al.*, 2022; Orr *et al.*, 2023). Studying these events thus requires subdaily meteorological observations. Such observations are available from Signy station for the period 1947–1995 and at Orcadas station from 1956 to the present (with quality-controlled data currently available up to May 2020). However, the records at Signy have only recently become available for scientific research as previously many of them just existed in paper-based form, which have only been digitised and quality-controlled of late by a team at the British Antarctic Survey. The newly digitised and quality-controlled Signy records overlap with the Orcadas records for the period 1956–1995, which provides an unprecedented opportunity for studying the spatiotemporal variation of extreme temperature events in the SOIs. Systematically examining both these datasets together for this common period allows us to better understand how the local orography, especially Coronation

Island, interacts with circulation anomalies to generate warm-temperature extremes in this region.

Here, for the first time, we investigate the seasonal and regional variation of extreme warm-temperature events and associated long-term trends in the SOIs using these observations from Signy and Orcadas stations. The large-scale circulation anomalies (and occurrence of ARs) associated with these extremes are studied using atmospheric reanalysis data. Finally, a high-resolution regional atmospheric model is used to investigate the detailed influence of the SOIs' orography on temperature, precipitation, and winds, and in particular the importance of föhn events in producing extreme warm temperatures at Signy station.

2 | DATA AND METHODS

2.1 | Station observations

Temperature observations from Orcadas station (60°44'24" S, 44°44'24" W) for the period 1956–2019

are available at six-hourly temporal resolution and have already undergone rigorous quality control as part of the SCAR READER project (Turner *et al.*, 2004). A similar quality control procedure was applied to the Signy station records (60°43'0" S, 45°36'0" W), which involves undertaking a detailed search for erroneous or potentially suspect data points (such as outliers and from unrealistic sudden changes). Such points were identified statistically, as well as by comparing the measurements with climatological values, records from nearby Orcadas station, and values from ERA5 reanalysis (Hersbach *et al.*, 2020). The suspect data points identified were subsequently checked by comparing with the original weather reports and the corresponding thermograms, and were subsequently corrected or removed.

The Signy records cover the period 1947–1995 with temporal resolution varying from one-hourly to daily, consisting of six-hourly data during 1947–1949, three-hourly from 1950 to 1974, 12-hourly during 1975, daily (at 1200 UTC) from 1976 to 1981, 12-hourly from 1982 to 1983, six-hourly from 1984 to 1987, and one-hourly from 1988 to 1995. However, data from Signy station for 1995 are excluded as during this period the instruments were not regularly maintained and the measurements are consequently considered unreliable; for example, annual mean temperature at Signy being 2°C lower than that at Orcadas in 1995.

2.2 | Identification of extreme warm-temperature events

Extreme warm-temperature events at Signy and Orcadas stations are determined as those exceeding the 95th percentile of the temperature histogram, based on all available observations at the standard synoptic hours of 0000, 0600, 1200 and 1800 UTC from the full datasets, that is, 1947–1994 for Signy and 1956–2019 for Orcadas. The 10 warmest events recorded at Signy and Orcadas stations during summer and winter are investigated in detail. Temperature thresholds based on the 95th percentile of all available observations for the common period of 1956–1994 are also calculated and compared with those based on the full records.

We also examine the variability and trends of warm-temperature events at both locations by examining the time series of the number of warm events occurring each year (again based on all available observations) relative to the total number of available observations, with warm events again defined as those equal to or exceeding the 95th percentile threshold (based on all months). We use an ordinary least-squares regression technique to estimate trends and the non-parametric Mann–Kendall

test to calculate trend significance (Alexander and Arblaster, 2009), which has been widely used for evaluating the presence of monotonic trends and makes no assumption for normality of the distribution.

2.3 | Reanalysis data

We use ERA5 reanalysis data (Hersbach *et al.*, 2020) to study the large-scale circulation anomalies associated with extreme warm temperatures at Signy and Orcadas stations. ERA5 has a horizontal grid spacing of 30 km and 137 levels in the vertical with meteorological fields available every hour from 1959 onwards. However, ERA5 fields are only well-constrained by satellite data from 1979 onward, as prior to this they are characterised by large uncertainties, especially for upper levels (Simmons and Hollingsworth, 2002; Marshall, 2003). We therefore only use ERA5 data from 1979 onwards. The ERA5 data used are 2-m temperature, 2-m relative humidity (required to calculate the 2-m dew-point temperature), mean-sea-level pressure (MSLP), 10-m zonal wind component, 10-m meridional wind component, as well as temperature, water vapour, zonal wind component, and meridional wind component on 37 pressure levels from 1,000 to 1 hPa.

To evaluate the large-scale drivers associated with the extreme warm anomalies, anomalies of MSLP and temperature at 850 hPa are estimated based on 31-day centred averages from ERA5 reanalysis for those days when at least one extreme warm event was observed at a given station during both summer and winter for the period 1979–1994, that is, from when reanalysis data are considered reliable. Note that we examined the sensitivity to the length of the running average window by examining periods of 15, 31 and 61 days (not shown). It is found that the general shape of the anomalies does not change with the length of the running window size, although there was a small change in amplitudes (e.g., the MSLP anomaly increased by 2 hPa from 15 to 61 days).

The fine-scale meteorological forcing features for the SOIs (such as föhn effects) are poorly represented in ERA5 because of the combination of the small horizontal extent of the islands and the limited horizontal resolution of the reanalysis, resulting in the islands being essentially unresolved as the ERA5 grid points corresponding to their location are treated as ocean and not land (e.g., Yuan, 2004; Alexander *et al.*, 2009; Hosking *et al.*, 2014). We expect this to result in a severe underestimation of föhn effects and the associated warming in ERA5, which in turn will lead to a misrepresentation of extreme temperatures (Bozkurt *et al.*, 2018). Other important land–atmosphere interactions will also therefore be misrepresented, such as the atmospheric boundary layer and turbulent fluxes, which

are dependent on surface roughness length (Hersbach *et al.*, 2020; Orr *et al.*, 2021).

2.4 | Identification of föhn conditions

To detect whether föhn conditions may have occurred during the top 10 warmest events we use the same surface criteria used by King *et al.* (2017), which required that over the six-hour period preceding the warm event (a) temperature increases, (b) wind speed increases, and (c) relative humidity decreases (with no thresholds applied for these criteria). For a given station, the upstream flow must impinge on regions of significant orography to cause föhn winds downstream. We thus adopt a further stipulation that the wind must be northerly or northwesterly at Signy and northwesterly or westerly at Orcadas. Note that if there are missing data values during any of the warm events then the criteria check is not performed for that event.

As an additional check, we also detect the occurrence of possible föhn conditions by using ERA5 data to compute the non-dimensional mountain height $\hat{h} = Nh/U$ for flow impinging on Coronation Island for each of the top 10 events that occur after 1979, where N is the buoyancy frequency, h is the mountain height ($= 1,200$ m), and U is the speed of the wind impinging on the island. Föhn conditions are associated with a non-linear flow regime, which occurs for $\hat{h} > 1$ (Orr *et al.*, 2004, 2008, 2021). Here, we define $N = \sqrt{(\mathbf{g}/\theta)(\Delta\theta/\Delta z)}$, where \mathbf{g} is the gravitational acceleration, θ is the potential temperature, $\Delta\theta$ is the difference in potential temperature at 700 and 950 hPa, and $\Delta z = 2,500$ m. To compute \hat{h} for Signy station, the value of U is based on the meridional wind speed at 950 hPa at the location of Coronation Island (i.e., $60^{\circ}37'S$, $45^{\circ}35'W$) at an altitude of around 500 m (or roughly the midpoint of the actual height of Coronation Island), while to compute \hat{h} for Orcadas station the value of U is based on the zonal wind speed at 950 hPa. Note that typically the value of U is based on the flow speed upstream of the orographic obstacle, but this is not applied here as the SOIs are essentially unresolved in ERA5. Furthermore, the value of N had to be computed for each event (also at the location of Coronation Island) as it was considerably larger than the typical value of 0.01 s^{-1} that is assumed for midlatitudes, that is, consistent with very stably stratified conditions, generated by warm air aloft being advected over the much colder surface of the Southern Ocean.

2.5 | Identification of atmospheric rivers

To detect whether ARs may have occurred during warm extremes at Signy and Orcadas stations, we firstly extract

the AR shapes/outlines of those having landfall from the AR database provided by Bin Guan via the Global Atmospheric Rivers Dataverse for the period of 1979–2019. This database identifies these ARs using the criteria of Guan and Waliser (2019), which required the following conditions to be met: (a) the integrated vapour transport (IVT) exceeds the 85th percentile of its seasonal mean and the total IVT within the feature is larger than $100 \text{ kg}\cdot\text{m}^{-1}\cdot\text{s}^{-1}$, and (b) the length of the IVT feature is more than 2000 km and its length/width ratio is above 2. Secondly, for the top 10 warmest events we also calculated the zonal and meridional components of the IVT at the time of the extremes. This is computed using ERA5 data on pressure levels as $Q_u = \int_{p_0}^p uq/g dp$ and $Q_v = -\int_{p_0}^p vq/g dp$ where u and v are the zonal and meridional winds, q is water vapour, and p is pressure. At a given grid point and time, the strength of the IVT is estimated as $\sqrt{Q_u^2 + Q_v^2}$.

2.6 | Regional atmospheric modelling

To clarify the influence of föhn events, we simulate a warm extreme case study of an event at Signy station using a high-resolution (1-km grid spacing) configuration of version 13.0 of the UK Met Office Unified Model (MetUM). The MetUM is a numerical weather prediction model based on the non-hydrostatic ENDGame (Even Newer Dynamics for General atmospheric modelling of the environment) dynamical core, which is solved by semi-implicit and semi-Lagrangian numerical methods (Wood *et al.*, 2014) on a regular (rotated) latitude–longitude grid. Our model setup is adapted from that used by Gilbert *et al.* (2020) and Orr *et al.* (2021) and uses the Regional Atmosphere physics configuration for midlatitudes (RA1M; Bush *et al.*, 2020).

The 1-km domain covers the SOIs and surrounding ocean, and uses orography derived from the 100-m resolution Radarsat Antarctic Mapping Project (RAMP) digital elevation model (Liu *et al.*, 2015), which gives a peak elevation of 1,006 m over Coronation Island (cf. actual peak height of 1,265 m). All domains have 70 vertical levels up to an altitude of 40 km, which comprises 16 levels within the lowest 1,000 m of the atmosphere (at 5, 22, 45, 75, 112, 155, 204, 261, 324, 394, 470, 553, 643, 739, 842 and 951 m above the surface).

Initial and boundary conditions for the outermost 12-km domain are supplied by a global version of the MetUM at N512 resolution ($1,024 \times 768$ grid points, equivalent to a horizontal resolution of ~ 25 km at midlatitudes), which is initialised with ERA5 data. The 12-km model is subsequently used to produce initial and boundary conditions for the 4-km model, which in turn produces initial and boundary conditions for the 1-km model. The model

is run twice-daily at 0000 and 1200 UTC to produce a series of 24-hour forecasts. The initial 12 hours of each forecast is discarded as spin-up, with the remaining part of the forecasts concatenated together to form a continuous time series. Only model output from the 1-km domain is analysed in this study as this resolution is necessary to realistically capture the detailed circulation and temperature features associated with föhn events (Orr *et al.*, 2021).

3 | RESULTS

3.1 | Observed temperature extremes

Figure 2 shows the normalised histogram of temperature observations for all months (black line) for Signy and Orcadas stations. Similar results are seen for the common period 1956–1994 (not shown). The temperature distributions at the two stations for all months are broadly similar. They are characterised by a peak around 0°C (i.e., the melting point of snow/ice), a left-skewed long cold tail (reaching as low as −40°C), and a much shorter warm tail (reaching as high as 20°C for Signy and around 14°C for Orcadas). Also shown for each station are histograms of temperature for summer and winter. As expected, the histograms for summer and winter broadly match the warm and cold tails of the histogram respectively, for all months for each station. For winter, both histograms are non-Gaussian and have a peak below the melting point of snow/ice, with Orcadas showing slightly more left skew and a steeper peak compared to Signy. For summer, both histograms show a largely Gaussian distribution and a peak above the

melting point of snow/ice, with Signy showing a slightly longer warm tail than Orcadas.

The number of extreme warm events for both Signy and Orcadas stations are given in Table 1, as well as the long-term averages and standard deviation of temperature, and the thresholds for the 95th percentile of the temperature distribution (also shown in Figure 2). Results are given for both the full datasets, as well as the common period of 1956–1994. Based on the full datasets, 2,976 extreme warm events for Signy station and 4,291 for Orcadas were identified for all months. The number of extreme warm events reduces to approximately 1,000 at Signy and approximately 1,400 at Orcadas for both austral summer (December to March) and austral winter (June to September). The average summer temperatures at Signy and Orcadas are similar and only just above the melting point of snow/ice (0.7°C at both locations during summer), while for winter and all months they are well below this threshold (−8.1°C for Signy and −7.8°C for Orcadas during winter, and −3.6°C and −3.3°C for all months). However, extreme warm-temperature thresholds for both Signy and Orcadas all exceed the melting point for all months, summer, and winter. Crucially, Table 1 and Figure 2 therefore suggest that warm extremes potentially play an important role in snow and ice melt at both locations. Moreover, thresholds are 1.2°C higher for Signy compared to Orcadas during summer (4.8°C compared to 3.6°C), 1.0°C higher during winter (1.5°C compared to 0.5°C), and 0.8°C for all months (3.5°C compared to 2.7°C). Thus, the thresholds are sensitive to location and Signy is generally characterised by higher temperature extreme events compared to Orcadas. For example, if we

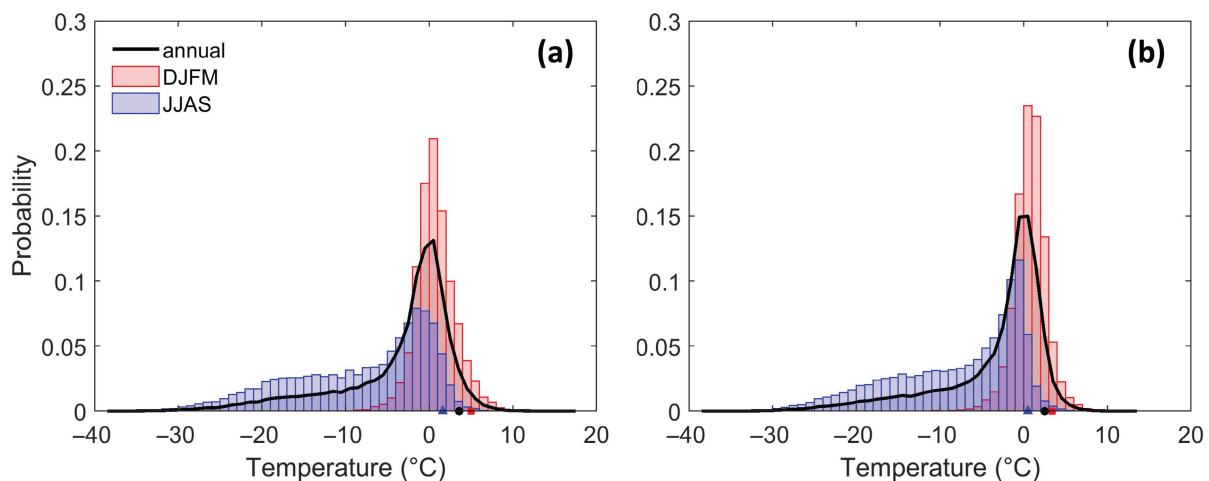


FIGURE 2 Normalised histograms of all available synoptic temperature observations for all months (black line) for (a) Signy station and (b) Orcadas station based on their full datasets (i.e., 1947–1994 and 1956–2019 respectively), as well as the corresponding histograms during summer (December–March, red) and winter (June–September, blue). The black circle, red square and blue triangle indicate the associated 95th percentile temperature thresholds for all months, summer and winter respectively. See Table 1 for exact values.

TABLE 1 The mean temperature (mean, °C), standard deviation (Std, °C), 95th percentile temperature thresholds (95th, °C), and total number of extreme warm events (*n*) for Signy and Orcadas stations based on all available synoptic observations for their full datasets (i.e., 1947–1994 and 1956–2019 respectively) for all months, summer (December–March), and winter (June–September). The corresponding values for the common period of 1956–1994 are shown in parentheses.

Station	All months				Summer				Winter			
	Mean	Std	95th	<i>n</i>	Mean	Std	95th	<i>n</i>	Mean	Std	95th	<i>n</i>
Signy	−3.6 (−3.5)	6.8 (6.8)	3.5 (3.6)	2,976 (2253)	0.7 (0.8)	2.4 (2.4)	4.8 (4.9)	980 (805)	−8.1 (−8.1)	8.2 (8.1)	1.5 (1.5)	1,003 (747)
Orcadas	−3.3 (−3.6)	6.3 (6.4)	2.7 (2.4)	4,291 (2580)	0.7 (0.5)	1.9 (1.9)	3.6 (3.4)	1,424 (788)	−7.8 (−8.0)	7.6 (7.7)	0.5 (0.4)	1,406 (788)

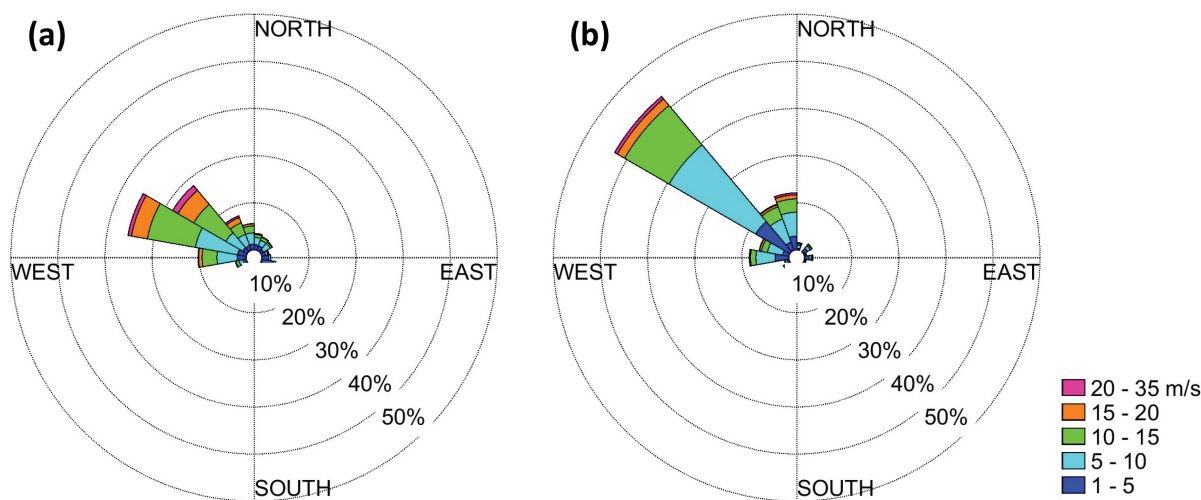


FIGURE 3 The 10-m wind rose for the extreme warm events based on observations from (a) Signy station and (b) Orcadas station, based on their full datasets (i.e., 1947–1994 and 1956–2019 respectively).

take 2.7°C as a reference warm-temperature threshold (i.e., the warm-temperature threshold for Orcadas station for all months), then the number of days per year on average with at least one observed synoptic temperature exceeding this is 18 for Orcadas station and 32 for Signy station (not shown). For the common period of 1956–1994, Table 1 shows that the number of extreme warm events is similar for both stations (e.g., 2,253 for Signy and 2,580 for Orcadas were identified for all months). Table 1 also shows that the temperature thresholds and other statistics for the common period of 1956–1994 are similar to the values for the full datasets for each station.

The wind direction measured at both stations during the warm extremes identified in Table 1 and Figure 2 is predominantly northwesterly, especially for Orcadas station (Figure 3). For example, 43% of the winds during the warm extremes at Orcadas come from the 300–320° E sector with wind speeds of 5–10 m·s^{−1} around 20% of the time and 10–15 m·s^{−1} around 10% of the time. The wind direction for both stations is therefore consistent with the warm events being induced by a combination of large-scale

advection of warm air from the north, as well as local amplification by föhn events (King *et al.*, 2017).

The 10 warmest independent extreme temperatures at the two stations are listed in Table 2 for summer and Table 3 for winter. As mentioned in the Introduction, during summer the warmest temperatures measured at Signy and Orcadas stations were 19.8 and 13.5°C (on 0000 UTC 30 January 1982 and 1800 UTC 23 December 1987 respectively). By contrast, during winter the warmest temperatures at Signy and Orcadas were 7.6 and 8.0°C (on 1200 UTC 22 September 1964 and 0000 UTC 2 June 2010 respectively). Tables 2 and 3 also show the wind direction during each of these events, which is broadly northwesterly for all instances, so consistent with the advection of relatively warm air towards the SOIs being a critical factor for the occurrence of warm extremes.

To detect whether föhn conditions may have occurred at the stations during the warm events, Tables 2 and 3 also include the corresponding values of wind speed, relative humidity and temperature observed at the time of each of the events, as well as six hours before each event. This

TABLE 2 The rank, time, date, temperature magnitude (T , °C), relative humidity (RH, %), 10-m wind speed (WS, m·s⁻¹), wind direction (WD, °E), and non-dimensional mountain height \hat{h} of the top ten warmest temperature events recorded at Signy (top rows; during 1947–1994) and Orcadas (bottom rows; during 1956–2019) stations for summer. The corresponding temperature, relative humidity, and wind speed values occurring six hours before each event are also given in parentheses. Missing values are indicated by N/A (e.g., relative humidity values are only available at Orcadas after 1987). Events with no missing values that likely involve föhn effects using the criteria that temperature and wind speed increase and specific humidity decreases over the preceding six-hour period are indicated by a diamond sign to the right of the time, date column. Events occurring after 1979 that involve föhn effects using the criteria that $\hat{h} > 1$ are indicated by a double diamond sign to the right of the time, date column. Events occurring after 1979 and involving the landfall of an AR during the 12 hours preceding the extreme warm event are indicated by a plus sign to the left of the time, date column.

Station	Rank	Time, date	T	RH	WS	WD	\hat{h}
Signy	1	+ 0000 UTC 30-Jan-1982◆◆	19.8 (13.6)	55 (80)	10 (3)	300	1.3
	2	+ 0000 UTC 13-Jan-1991◆	17.4 (13.1)	22 (40)	29 (21)	320	0.9
	3	1800 UTC 03-Jan-1974	12.9 (9.4)	N/A	11 (10)	330	N/A
	4	1800 UTC 05-Jan-1962◆	12.3 (5.3)	61 (85)	20 (10)	40	N/A
	5	+ 1800 UTC 26-Jan-1985◆◆	12.0 (2.8)	N/A	8 (2)	N/A	2.0
	6	+ 1800 UTC 11-Mar-1990	11.9 (5.1)	56 (97)	17 (20)	290	1.3
	7	+ 1200 UTC 14-Feb-1994◆◆	11.7 (5.3)	73 (100)	13 (33)	310	1.3
	8	+ 1800 UTC 18-Dec-1994◆◆	11.7 (7.4)	42 (34)	21 (11)	310	1.1
	9	+ 0000 UTC 24-Dec-1987◆◆	11.6 (8.0)	N/A	27 (28)	290	7.7
	10	0600 UTC 30-Dec-1988◆◆	11.6 (9.4)	61 (46)	25 (15)	340	8.9
Orcadas	1	+ 1800 UTC 23-Dec-1987◆	13.5 (5.0)	57 (84)	20 (8)	340	0.7
	2	+ 0000 UTC 26-Jan-1995◆◆◆	11.7 (8.4)	70 (83)	20 (14)	270	1.1
	3	+ 1800 UTC 19-Jan-2006◆◆◆	11.6 (3.4)	79 (89)	10 (8)	320	1.7
	4	+ 1800 UTC 11-Feb-1995	11.4 (7.6)	49 (80)	25 (16)	250	0.8
	5	+ 1800 UTC 24-Feb-2018	10.7 (8.7)	69 (77)	13 (18)	340	0.8
	6	1800 UTC 29-Feb-1960	9.6 (0.0)	N/A	13 (13)	320	N/A
	7	+ 1800 UTC 23-Jan-1997◆◆	9.4 (2.9)	77 (73)	10 (18)	180	1.6
	8	+ 1800 UTC 14-Dec-2001	9.3 (5.4)	29 (65)	18 (20)	320	0.7
	9	+ 1800 UTC 04-Mar-1997◆	9.2 (6.9)	57 (77)	16 (10)	320	1.1
	10	+ 1800 UTC 25-Jan-1992◆◆	9.1 (7.4)	N/A	23 (14)	320	1.3

Abbreviations: RH, relative humidity; T , temperature magnitude; wd, wind direction; ws, 10-m wind speed.

shows that three out of seven summer events and five out of nine winter events at Signy station show some indication of föhn conditions, that is, upstream flow impinging on orography from a northerly or northwesterly direction, as well as strengthening winds, warming, and drying at the leeside surface (Elvidge *et al.*, 2015, 2016; Elvidge and Renfrew, 2016; King *et al.*, 2017; Orr *et al.*, 2008, 2021, 2023; Gilbert *et al.*, 2022). Tables 2 and 3 show that at Orcadas station, four out of eight and four out of six events in summer and winter respectively exhibit some indication of föhn conditions using these criteria based on station data. Note that only events with no missing data values were included in this comparison, which is why the sample size considered here is less than 10.

These findings are largely in agreement with estimates of the occurrence of föhn conditions based on the value of \hat{h} for each of the events occurring after 1979 (Tables 2 and 3), that is, \hat{h} is larger than 1. This suggests that seven out of eight summer events and four out of six winter events at Signy station show some indication of föhn conditions, compared to five out of nine summer events and one out of seven winter events at Orcadas station, that is, more incidences of föhn conditions at Signy station compared to Orcadas station.

To explore the variability and trends of warm extreme temperature events in the SOIs, Figure 4 shows the time series of the percentage of the number of temperature observations each year that are either equal to or are

TABLE 3 Same as Table 2 except for winter.

Station	Rank	Time, date	T	RH	WS	WD	\hat{h}
Signy	1	1200 UTC 22-Sep-1964♦	7.6 (2.3)	54 (77)	32 (29)	270	N/A
	2	+ 0000 UTC 17-Jul-1983♦♦	7.3 (−5.5)	62 (90)	28 (3)	320	1.2
	3	+ 0600 UTC 30-Sep-1980♦♦	6.5 (−1.3)	100 (100)	6 (0)	N/A	1.4
	4	1800 UTC 30-Sep-1962♦	6.2 (1.9)	48 (87)	25 (3)	280	N/A
	5	+ 0000 UTC 11-Jul-1986♦♦	6.2 (−4.5)	95 (100)	25 (24)	310	1.5
	6	+ 0000 UTC 31-Aug-1986♦	5.8 (1.5)	95 (98)	45 (16)	340	0.8
	7	+ 0600 UTC 26-Sep-1985	5.8 (2.1)	N/A	45 (19)	N/A	0.7
	8	0600 UTC 06-Sep-1957	5.7 (0.9)	55 (97)	28 (30)	290	N/A
	9	+ 0000 UTC 22-Aug-1984	5.7 (2.2)	80 (88)	30 (32)	300	1.1
	10	1800 UTC 22-Jun-1966	5.6 (3.4)	83 (78)	10 (10)	110	N/A
Orcadas	1	0000 UTC 02-Jun-2010♦♦	8.0 (0.0)	70 (91)	20 (20)	320	1.3
	2	0600 UTC 29-Sep-1962	7.5 (1.8)	N/A	26 (20)	320	N/A
	3	+ 1200 UTC 18-Jun-1981	6.4 (−0.4)	N/A	28 (15)	50	0.9
	4	0000 UTC 30-Aug-2003♦	6.3 (1.0)	62 (78)	18 (5)	290	0.8
	5	+ 1800 UTC 04-Sep-2016	6.3 (−2.3)	82 (82)	22 (25)	320	0.6
	6	0000 UTC 28-Jul-1958	6.0 (3.1)	N/A	22 (15)	320	N/A
	7	+ 1800 UTC 24-Sep-1996♦	6.0 (1.8)	79 (92)	12 (10)	290	0.9
	8	1800 UTC 19-Sep-2005	6.0 (0.6)	70 (94)	6 (10)	320	0.7
	9	1800 UTC 27-Aug-1969	5.8 (−1.8)	N/A	20 (25)	340	N/A
	10	0600 UTC 23-Jul-1992♦	5.7 (−4.0)	66 (91)	32 (26)	290	0.7

Abbreviations: RH, relative humidity; T , temperature magnitude; wd, wind direction; ws, 10-m wind speed.

greater than the 95th percentile temperature threshold for Signy and Orcadas (i.e., 3.5 and 2.7°C respectively; see Table 1). Statistically significant positive trends are detected at both stations, with a steeper increase at Signy compared to Orcadas. At Signy the trend is $0.95 \pm 0.2\%$ per decade ($p \leq 0.01$) during 1947–1994, and $0.74 \pm 0.2\%$ per decade ($p \leq 0.01$) during 1956–2019 at Orcadas.

Figure 5a shows a scatterplot of the observed warm-temperature extremes at Signy station against the corresponding concurrent observed temperatures at Orcadas station for the common period of 1956–1994. For 90% of the warm events at Signy, the temperatures at Signy are higher than at Orcadas, with an average difference of 3.3°C. By contrast, only 57% of the warm events at Orcadas are associated with temperatures that are higher than at Signy, with an average difference of 0.94°C (Figure 5b). These relationships between high temperatures at one station and the associated temperature at the other station are also weakly correlated (r values of 0.19 and 0.07). This suggests that warm extreme temperatures over the SOIs involve considerable spatial and temporal heterogeneity, with warm extremes at Signy station being especially localised compared to those at Orcadas station, suggesting

that föhn processes may be especially important at this location.

Figure 5c shows a scatterplot of observed temperature extremes against corresponding ERA5 temperatures at Signy station for 1979–1994. As expected, ERA5 substantially underestimates the temperatures of these warm events (by 4.0°C on average). Similarly, Figure 5d shows that ERA5 also underestimates Orcadas extreme temperatures, although less severely than for Signy (2.2°C on average).

3.2 | Synoptic drivers

Figure 6a shows the average MSLP anomalies based on 31-day centred averages from ERA5 reanalysis for those days when at least one extreme warm event was observed at Signy station during summer for the period 1979–1994, that is, from when reanalysis data is considered reliable. This is marked by a distinctive east–west dipole pattern centred over the SOIs, with negative anomalies reaching 6 hPa to the west of the islands over the Bellinghausen Sea and Drake Passage and positive anomalies

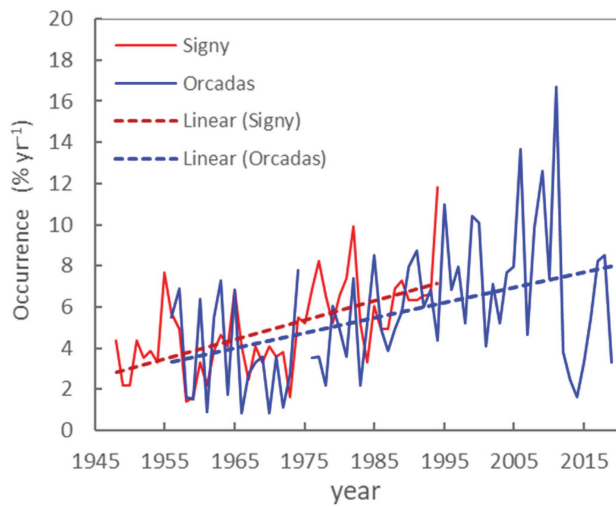


FIGURE 4 Time series (solid) and associated linear trends (dashed) of the percentage of the number of synoptic temperature observations each year ($\% \text{ yr}^{-1}$) that are either equal to or are greater than the 95th percentile temperature threshold for Signy (red) and Orcadas station (blue) based on data from all months. Warm events are defined as occasions when temperatures are equal to or exceeding the 95th percentile thresholds of 3.5°C for Signy station and 2.7°C for Orcadas station (see Table 1).

reaching 10 hPa to the east of the islands over the Southern Atlantic Ocean (centred at $20\text{--}35^{\circ}\text{W}$, $60\text{--}55^{\circ}\text{S}$), with the high-pressure anomalies over the Southern Atlantic Ocean acting to block the passage of eastward propagating low-pressure systems from the Drake Passage that channel warm and moist air masses towards the SOIs. These MSLP anomalies suggest that the extreme warm events at Signy are associated with enhanced northerlies, which would advect relatively warm air from lower latitudes towards the SOIs as well as induce localised föhn winds at Signy through their interaction with Coronation Island. These MSLP anomalies are in the range of 75th to 90th percentiles of the 31-day-running-average-based daily MSLP anomalies at the corresponding locations (cf. Figure S1).

The equivalent results for the warm extremes at Orcadas station during summer (Figure 6b) also show a dipole pattern, although this is relatively weaker and aligned more north–south compared to those for Signy station. This dipole pattern of MSLP anomalies is again consistent with enhanced northwesterlies/westerlies that advect warm air from the Drake Passage, as well as flow over Coronation Island with possible local föhn enhancement also being a possible critical factor. This pattern is broadly in agreement with the results found by Turner *et al.* (2021) who considered warm extremes based on year-round data during the period of 1979–2019.

Moreover, we find that during the warm extremes when Signy was warmer than Orcadas, the anomalous

MSLP also shows a west–east-oriented dipole pattern (not shown), that is, similar to what has been shown in Figure 6a. Conversely, for those warm extremes when Orcadas temperature was higher than that at Signy, the north–south orientation of the dipole pattern stands out (not shown), that is, the MSLP anomalies are similar to what has been shown in Figure 6b.

The composite MSLP anomalies for winter warm extremes at Signy and Orcadas are shown in Figure 6c,d. The pressure anomaly patterns near the SOIs are broadly similar to those in summer but they are generally 2–3 hPa larger. Thus, the extreme wintertime warm extremes in the SOIs involve deepened MSLP anomalies with enhanced northerlies at Signy and northwesterlies/westerlies at Orcadas. For both stations, these winter MSLP anomalies are consistent with a wave train originating from the extratropical Southern Pacific. It is likely that the larger amplitudes during winter are linked to the poleward shift of the baroclinic zone and thus the storm tracks during this season (Trenberth, 1991; Hoskins and Hodges, 2005).

Furthermore, we find that the annual percentage occurrence of SOIs' warm extremes and their associated trends (Figure 4) are statistically linked to the annual percentage occurrence of the differences in the MSLP anomaly dipole patterns shown in Figure 6. Figure 7 shows the percentage of the days per year when the differences between the positive and negative MSLP anomalies exceed 16 hPa for Signy and 12 hPa for Orcadas, which corresponds approximately to the MSLP differences between the positive and negative pressure anomalies shown in Figure 6a,b for each station. See the figure caption for the exact locations where the MSLP differences are computed based on the areal averaged daily mean MSLP anomalies. It is evident that the percentage of days per year associated with a daily difference MSLP value of 16 hPa or higher for Signy show a significant positive trend of $0.5 \pm 0.1\%$ per decade ($p < 0.001$). The percentage of days per year associated with a daily difference MSLP value of 12 hPa or higher for Orcadas also shows a positive trend of $0.6 \pm 0.2\%$ per decade ($p < 0.001$). Similar positive trends can also be obtained using any threshold values between 12 and 17 hPa, which roughly correspond to the 80th to 90th percentiles of the daily mean MSLP differences between the two dipole regions at both stations (not shown). At Signy station, the correlation between this difference in MSLP time series (Figure 7) and the annual percentage occurrence of warm extremes observed (Figure 4) is in the range of 0.46 to 0.53 ($p \leq 0.01$) for the period 1959–1994 depending on the threshold values taken for the MSLP differences, that is, in the range of 12–17 hPa, while for Orcadas station, the correlation between the difference in MSLP time series and the percentage occurrence-of-extremes time series is in the range

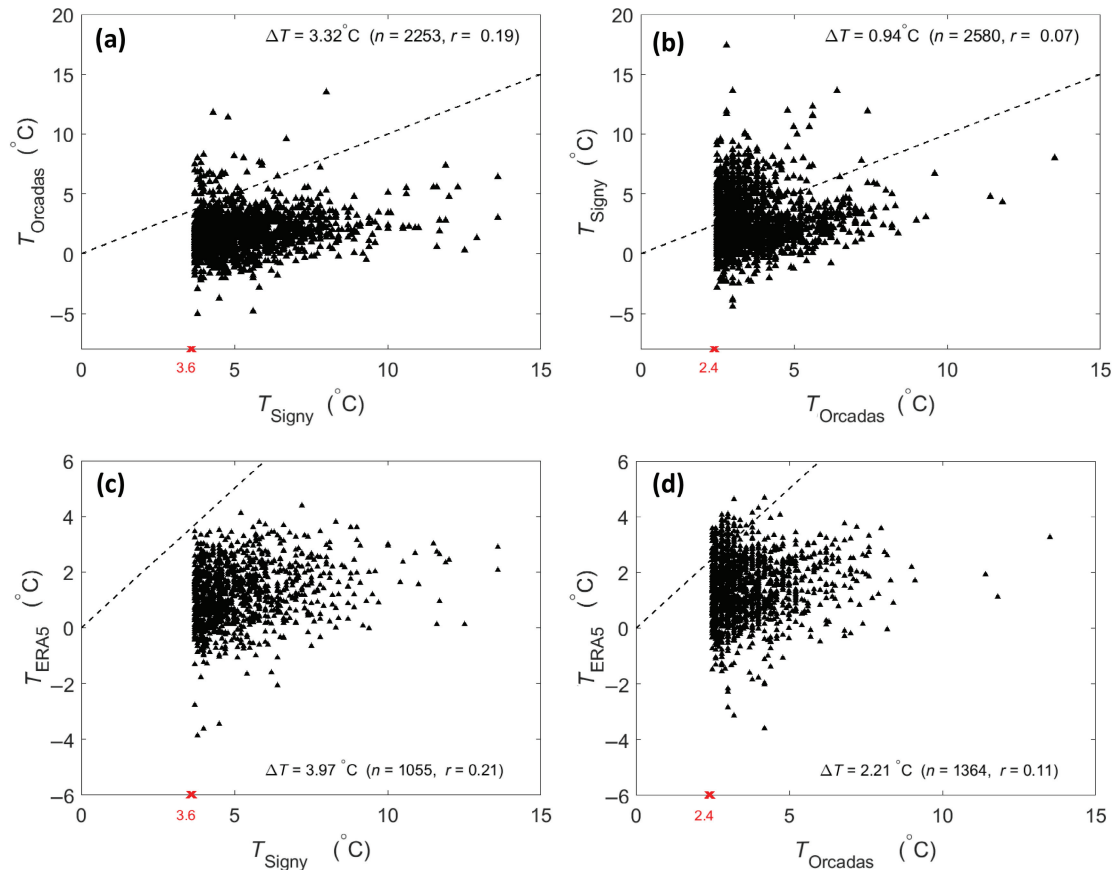


FIGURE 5 (a) Scatterplot of the extreme warm temperatures observed at Signy station and the corresponding co-occurring temperatures observed at Orcadas station for the common period of 1956–1994. Also shown for these events is the corresponding average temperature difference between the two stations (ΔT), the number of extreme events that occurred (n), and the correlation coefficient between the temperature differences (r). The threshold temperatures used to estimate the extremes are marked by the red cross at the x-axis. The dashed line is the reference 1:1 line. (b) Same as (a) except comparing extreme warm temperatures at Orcadas station with the corresponding temperatures observed at Signy station. Panels (c, d) are the same as (a, b) except that the extreme warm temperatures observed at the stations are compared with corresponding values from ERA5, but only for the period 1979–1994.

of 0.49 to 0.59 ($p \leq 0.0001$) for the period 1959–2019. These correlation coefficients remain statistically significant but reduce to just below 0.5 when the data are first detrended before performing the correlations. Thus, about 25% of the interannual variance in the station warm extreme occurrence may be explained by variations in the frequency of occurrence of a strong MSLP dipole pattern.

Figure 8a depicts composite temperature anomalies at 850 hPa derived from ERA5 centred 31-day running averages for those days when at least one extreme warm event was observed at Signy station for the period 1979–1994 during the summer months. The temperature anomalies are marked by warm anomalies that extend from the east coast of South America to the SOIs, with a maximum of 4°C over the extended area that covers the SOIs. For the warm extremes at Orcadas station (Figure 8b), the corresponding large-scale temperature anomalies are broadly similar to those associated with Signy but extend

over a smaller region and have a smaller peak of 3°C. These temperature anomalies agree well with enhanced northerlies and northwesterlies/westerlies during Signy and Orcadas warm extremes respectively (Figure 6). Also, the temperature anomalies associated with both stations show evidence of a wave train over the West Antarctic sector and the latitude band of 35–75° S. Broadly similar large-scale temperature anomalies can be found in winter warm extremes at Signy and Orcadas (Figure 8c,d). The only notable difference is that the magnitude of the temperature anomalies is typically larger (e.g., the positive temperature anomaly increases to 5°C). It is also worth noting that warm extremes at both stations correlate with ERA5 temperatures at approximately 850 hPa more significantly and with higher correlation coefficients than with 2-m temperatures, that is, r increases from approximately 0.25 to 0.5 for year-round data (not shown).

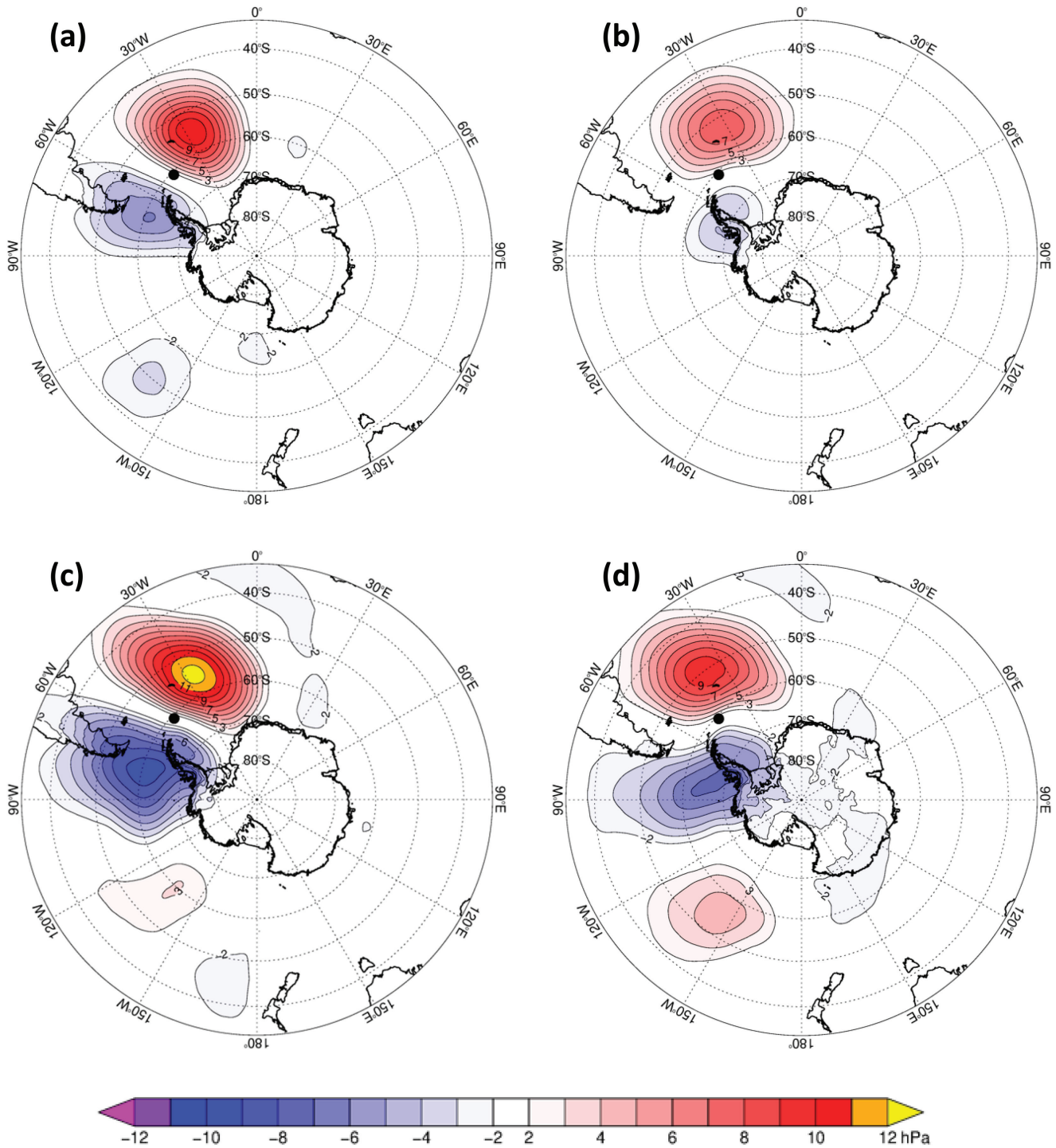


FIGURE 6 Composite of ERA5-based, 31-day centred mean-sea-level pressure (MSLP, hPa) anomalies for those days when at least one extreme warm-temperature event occurred at Signy (a, c) and Orcadas (b, d) stations in summer (a, b) and in winter (c, d) during 1979–1994. The station location is indicated by the black dot. All anomalies above or below ± 2 hPa are statistically significant at $p < 0.05$. The warm extreme events are determined by the threshold values listed in Table 1 for summer and winter.

Figure 9 shows mean temperature profiles and their standard deviation from ERA5 at Coronation Island during periods when extreme warm events were recorded at Signy and Orcadas stations in summer and winter (for the

period 1979–1994). The mean profiles associated with extreme high temperatures are substantially warmer than the climatology and are separated from the mean by at least one standard deviation. For both stations the mean

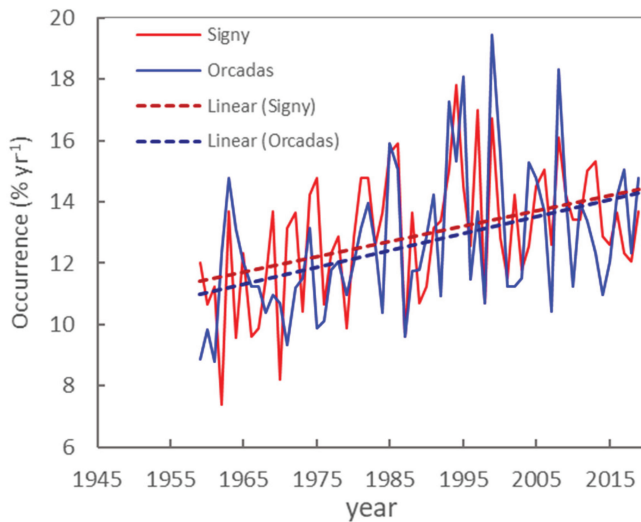


FIGURE 7 Time series of the percentage of the days per year ($\% \text{ yr}^{-1}$) when the mean-sea-level pressure (MSLP) anomaly differences of the dipole patterns of Figure 6a exceed 16 hPa (solid red line), where the daily-mean MSLP anomalies are estimated based on 31-day centred running averages and then areal-averaged over a box over the positive anomaly (at 20–40° W, 45–65° S) and a box over the negative anomaly (at 60–90° W, 45–65° S). The solid-blue line is the same except for the MSLP anomaly differences between the dipole pattern shown in Figure 6b exceeding 12 hPa, where the daily-mean MSLP anomalies are areal-averaged over a box over the positive anomaly (at 15–45° W, 45–65° S) and a box over the negative anomaly (at 60–90° W, 45–65° S). The associated linear trends of the time series are shown as the dashed lines.

profile is around 4–5°C warmer than the climatology during summer, and 6–7°C during winter. During summer, the differences in temperature compared to the climatology are also reduced at the near-surface compared to higher elevations. These results suggest that anomalously large-scale high temperatures aloft may play an important role in inducing station extremes. This is especially apparent for the profiles corresponding to the top three extreme warm events, which are between 10 and 20°C warmer than the climatology.

The temperature profiles for the top three extreme events also show pronounced near-surface inversions, especially during summer, which can form due to warm-air advection occurring aloft (King *et al.*, 2017; Orr *et al.*, 2021). This suggests that erosion of the inversion is necessary for the warm extremes to occur at the surface, which, as these events likely involve föhn effects (see Table 2), could occur from the downslope föhn winds descending the leeside of the mountain barrier and inducing enhanced turbulent mixing (Elvidge and Renfrew, 2016; Orr *et al.*, 2008, 2021). However, as previously mentioned, we would not expect ERA5 to capture föhn effects over the SOIs.

3.3 | Atmospheric rivers

Table 2 shows that seven out of eight of the top 10 extreme warm events that occurred after 1979 in summer at Signy involved an AR making landfall at the SOIs within 12 hours of the event, while for Orcadas this was nine out of nine of the top 10 summer events. Analogous results for winter shows that six out of six of the top 10 warm events involved an AR event at Signy, and three out of seven at Orcadas (Table 3). Note that only events that occurred after 1979 are included in this comparison, which is why the sample size considered here is less than 10. For all months, 36% of the Signy warm extremes involve an AR making landfall at the same synoptic hour (during 1979–1994), while for Orcadas warm extremes this occurs 27% of the time (during 1979–2019) (Table 4). In terms of seasonal variation, 41% of Signy extreme warm events in summer coincide with landfalling ARs at the same synoptic hour, which reduces to 27% at Orcadas. Similarly, 52% of Signy winter extreme warm events coincide with landfalling ARs at the same synoptic hour, which reduces to 38% at Orcadas. However, when the measure of landfalling ARs includes the 12 hours before the event, the difference between the two stations become small, with warm extremes at both stations involving ARs 48% of the time for all months, 52% of the time for summer, and around 60% for winter (Table 4). These results suggest that the ARs are likely responsible for the substantially warmer than average temperature profiles at the location of Coronation Island that are associated with extreme warm events (Figure 9).

Figure 10 shows IVT anomalies associated with the top two extreme warm events at Signy (i.e., on 0000 UTC 30 January 1982 and 0000 UTC 13 January 1991), which both involved landfall of ARs (Table 2). Both of these events involve an AR stretching from off the east coast of South America all the way to the SOIs, that is, characterised by pronounced southward transport of moisture. In both cases the AR (or at least a branch of it) appears to originate from the Southern Pacific, before crossing over the Andes/South America, and thereafter gaining moisture over the Brazil-Falkland Confluence zone/Southern Ocean, that is, the region of water off the coast of South America between 50–70° W and 35–45° S that is known to be dynamically active and complex (Peterson and Stramma, 1991). Additionally, the transport of large amounts of moisture from low to high latitudes by the South American low-level jet might also play an important role (Montini *et al.*, 2019; Ramos *et al.*, 2019).

Figure 10 also shows the MSLP and 10-m wind anomalies associated with these two events, which show broadly consistent large-scale patterns. These consist of (a) an elongated ridge of anomalously high pressure to the east of

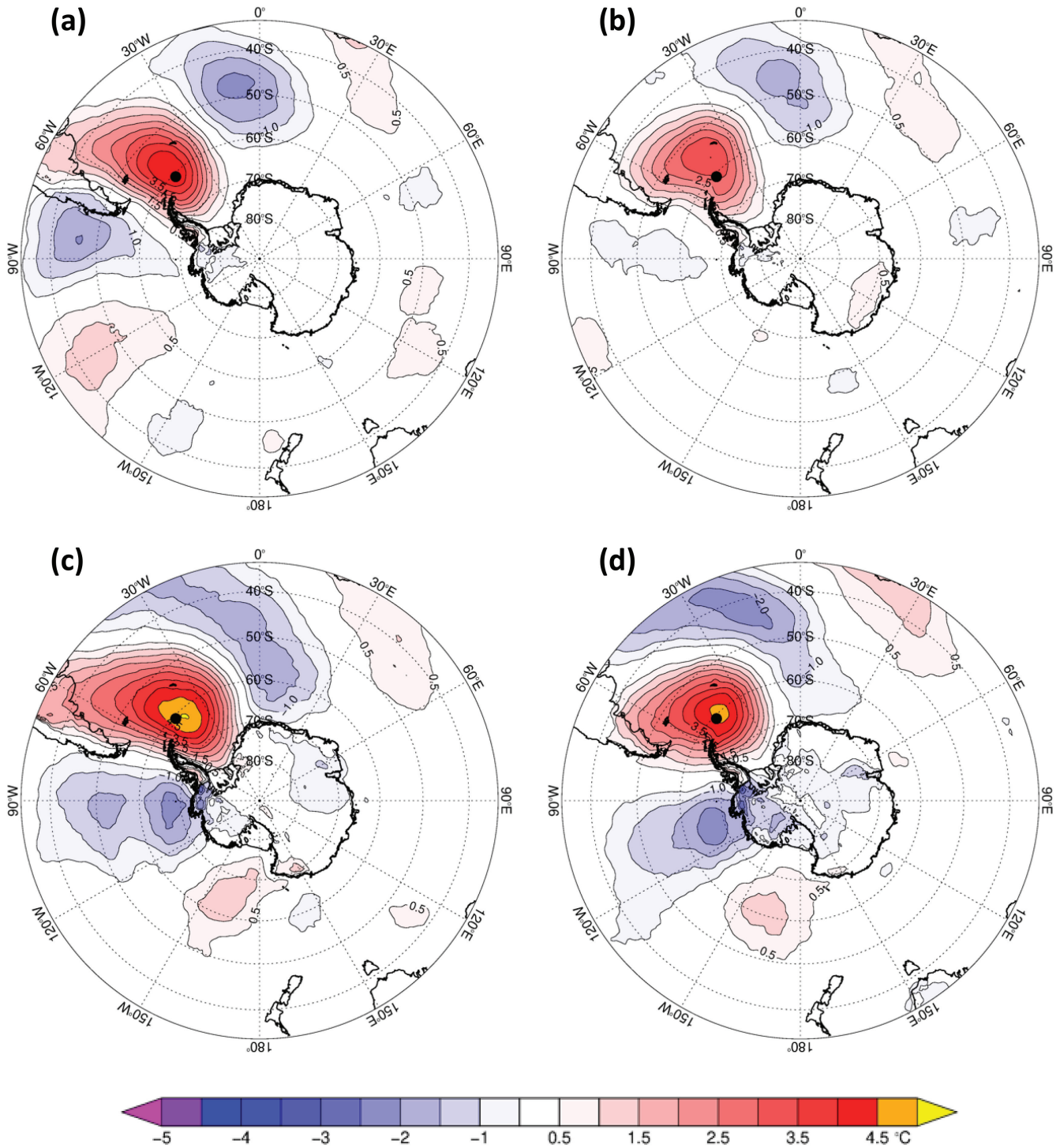


FIGURE 8 Same as Figure 6 except that the mean-sea-level pressure (MSLP) anomalies are replaced by temperature anomalies at 850 hPa.

the SOIs, extending southward from the Southern Atlantic Ocean towards the Weddell Sea, (b) a trough of anomalously low pressure to the west of the SOIs, connecting low-pressure areas located around the Antarctic Peninsula and off the west coast of South America, and (c) an elongated region of pronounced anomalous northerly winds of about $10 \text{ m}\cdot\text{s}^{-1}$ stretching from the east coast

of South America to the SOIs, that is, consistent with the pronounced southward transport of moisture. These MSLP patterns are broadly in agreement with the distinct east–west dipole pattern in MSLP anomalies for those days when at least one extreme warm event was observed at Signy station (Figure 6a). Similar IVT, MSLP, and 10-m wind anomalies to these were also found for the other

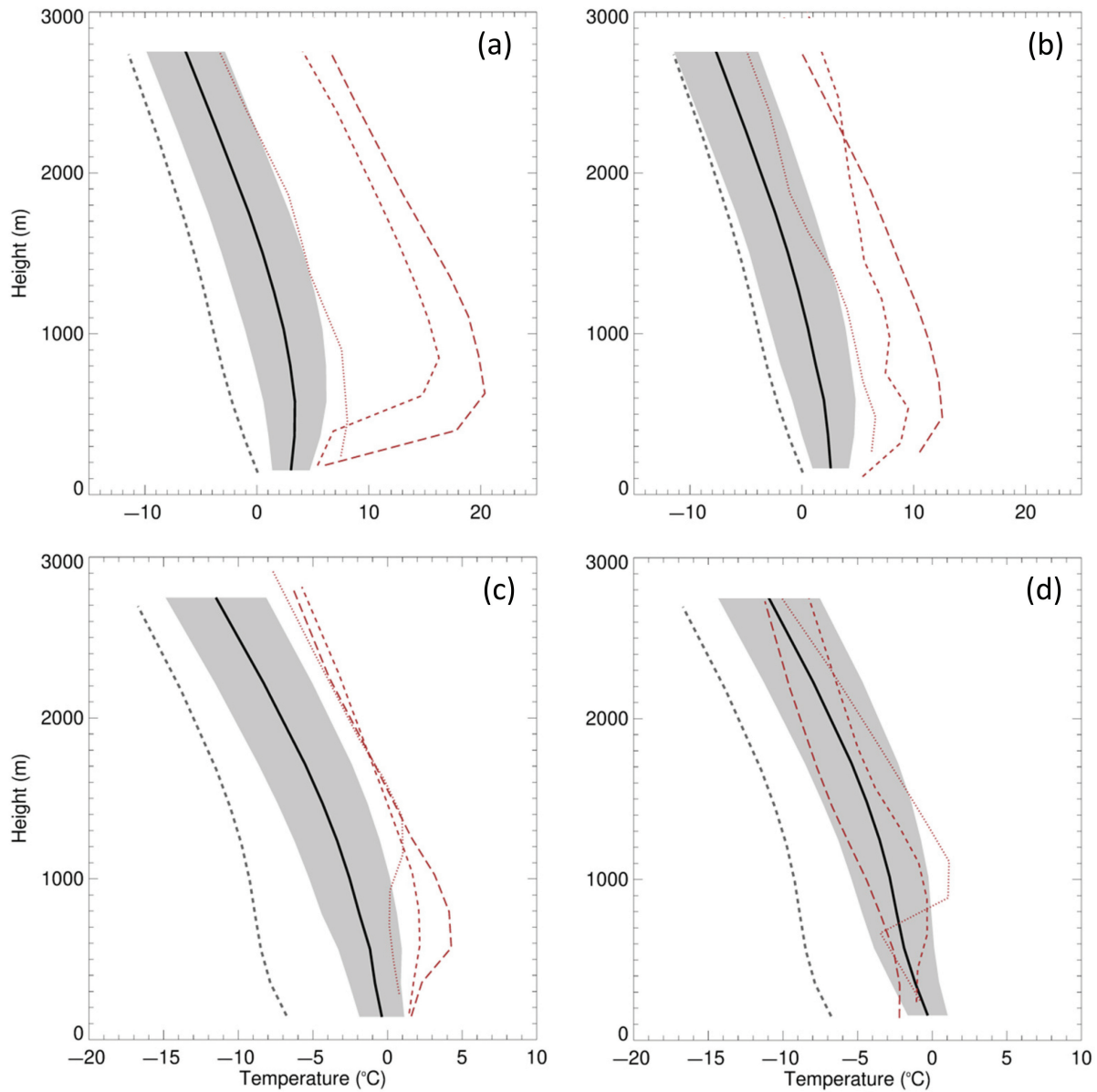


FIGURE 9 Vertical profiles of mean (black solid line) and standard deviation (grey shaded area) of temperature from ERA5 at 46.5° W, 60° S, which corresponds to the location of Coronation Island directly north of the Signy station and west of the Orcadas station, during the same times when extreme warm events were observed at Signy (a, c) and Orcadas (b, d) stations in summer (a, b) and in winter (c, d) for the period 1979–1994. Also shown is the climatological temperature profile (grey dashed line) and profiles of the top three warm events shown in Tables 2 and 3 (long red dashed, short red dashed, and dotted red lines). Note that top and bottom panels have different ranges.

TABLE 4 The percentage (%) of the warm extremes at Signy and Orcadas stations that involve landfalling atmospheric rivers at the same time of the event and 12 hours up to the event from 1979–1994 to 1979–2019 respectively. Results are shown for all months, summer, and winter.

Station	All months		Summer		Winter	
	Same time	12 h up to	Same time	12 h up to	Same time	12 h up to
Signy	36	48	41	52	52	66
Orcadas	27	48	27	52	38	57

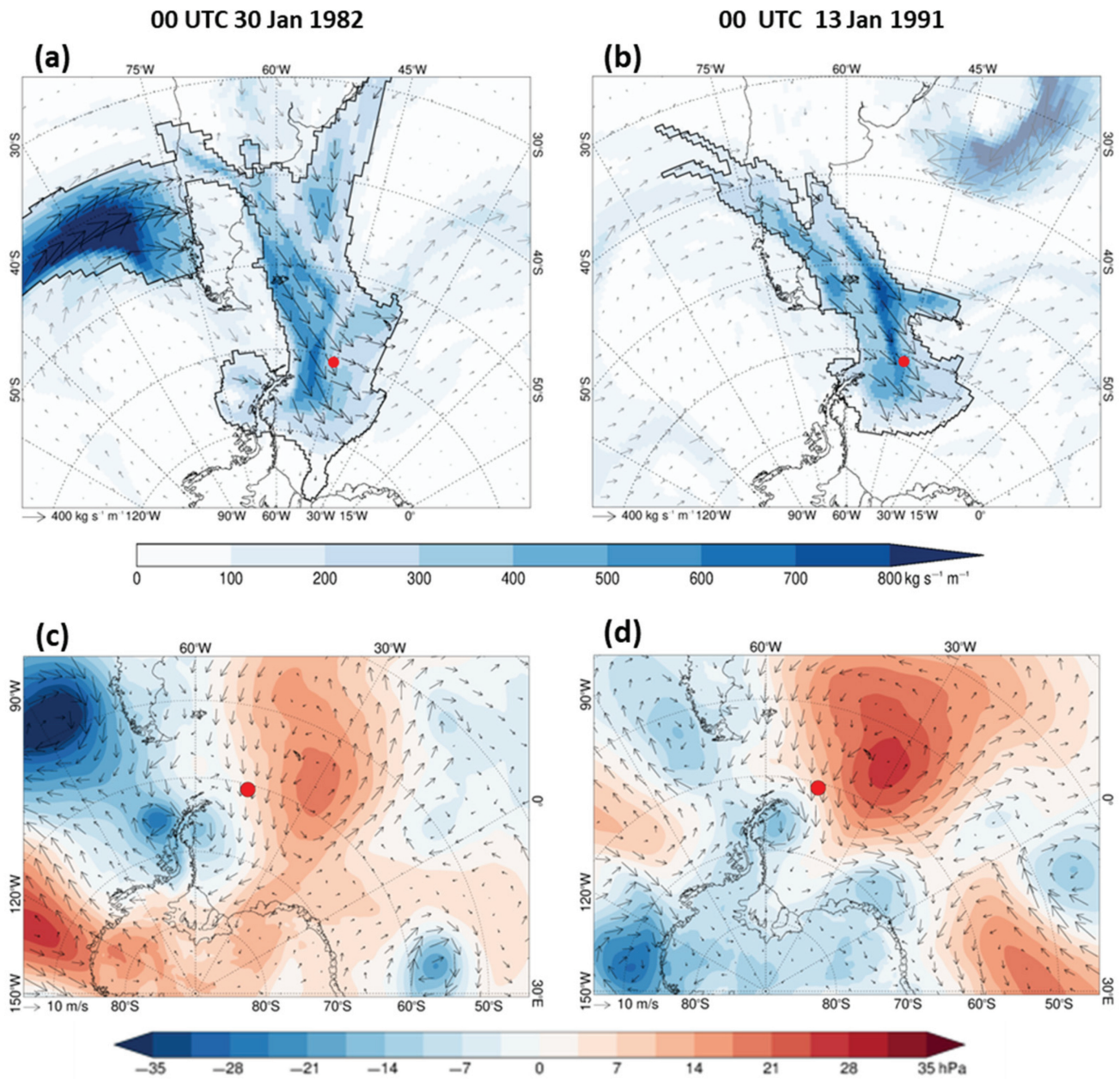


FIGURE 10 Anomalies of integrated vapour transport (IVT, $\text{kg}\cdot\text{m}\cdot\text{s}^{-1}$; arrows and shading) (a, b) and mean-sea-level pressure (hPa; shading) and 10-m winds ($\text{m}\cdot\text{s}^{-1}$, arrows) (c, d) associated with the top two extreme warm events after 1979 during summer at Signy (i.e., on 0000 UTC 30 January 1982 and 0000 UTC 13 January 1991), which both involved landfall of ARs (Table 2). In panels (a, b) the solid black line shows the spatial footprint of the AR based on the criteria outlined in Section 2.4 and Guan and Waliser (2019). The location of Signy station is shown by the red dot.

five top 10 summer extreme warm events occurring after 1979 at Signy (Table 2 and Figures S2 and S3). In particular, the IVT vectors and the 10-m wind anomalies tend to point south near the SOIs. The associated MSLP anomalies are also extreme in the sense that either the high-pressure centre exceeds the 90th percentile of its 31-day MSLP running-average-based anomaly or the low-pressure centre is well below its 10th percentile at the same location (cf. Figure S1).

Similarly, the circulation anomalies and the IVT morphology associated with the top two extreme warm events at Orcadas during summer are shown in Figure 11 (i.e., at 1800 UTC 23 December 1987 and 0000 UTC 26 January 1995), which also both involved landfall of ARs (Table 2). The first of these events involves an AR stretching from off the east coast of the South America/Brazil-Falkland Confluence zone over the Drake Passage and all the way to the Antarctic Peninsula (i.e., pronounced southward

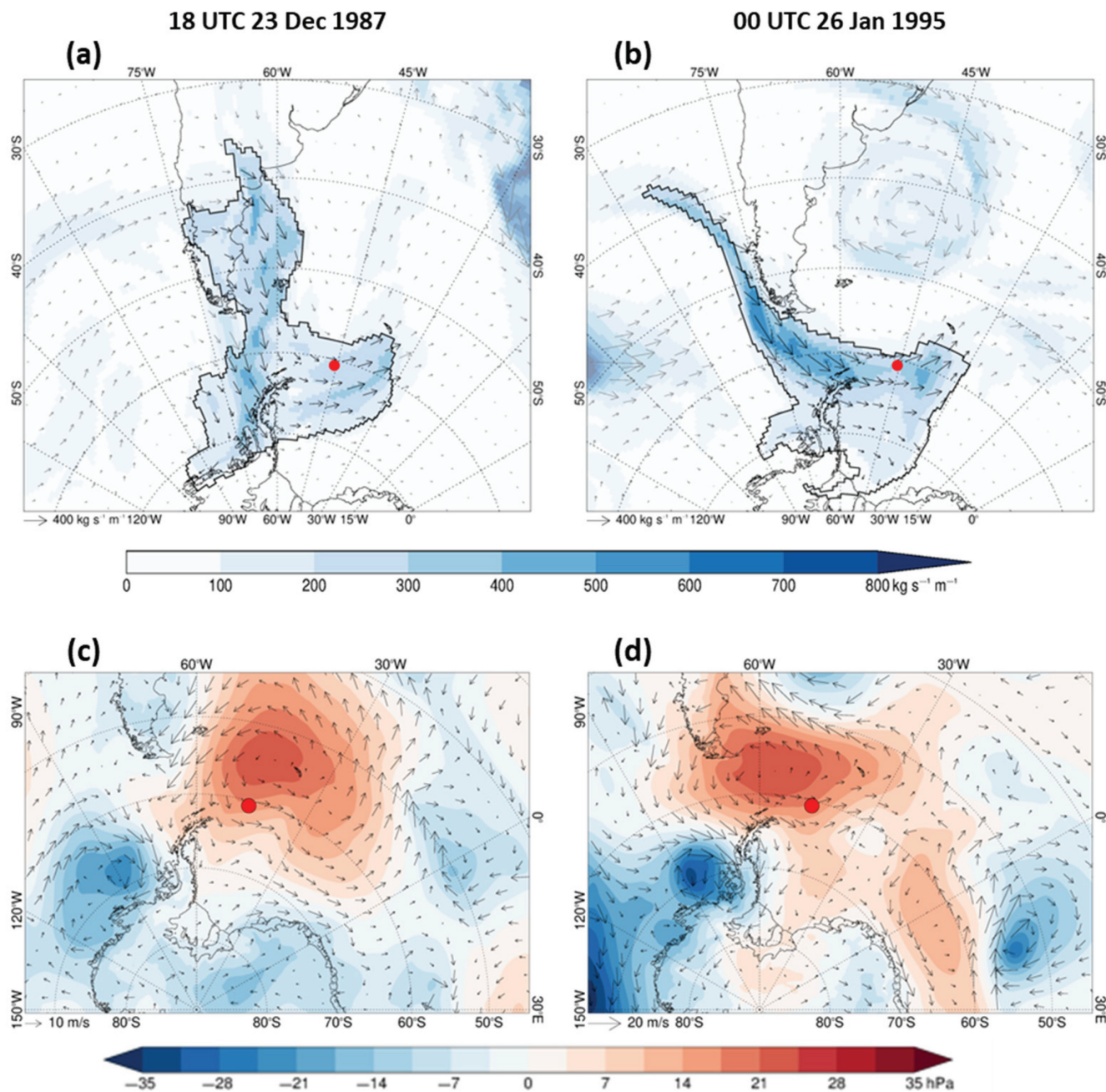


FIGURE 11 As in Figure 10, but for the top two extreme warm events at Orcadas station during summer, that is, at 1800 UTC 23 December 1987 and 0000 UTC 26 January 1995. The location of Orcadas station is shown by the red dot.

transport of moisture), with a branch of the AR veering to the east over the Drake Passage and reaching the SOIs. The second of these events involves the AR stretching from off the west coast of South America all the way to the Antarctic Peninsula (i.e., pronounced southeastward transport of moisture), with again a branch of the AR veering to the east over the Drake Passage and reaching the SOIs. These features are associated with broadly similar circulation anomalies, consisting of (a) a region of

high pressure located immediately north of the SOIs (over the Drake Passage/Brazil-Falkland Confluence zone), (b) a region of low pressure to the west of the Antarctic Peninsula, and (c) westerly/northwesterly flow of about 10 m s⁻¹ over the SOIs. These MSLP patterns agree well with the more east–west-oriented dipole for those days when at least one extreme warm event was observed at Orcadas station (Figure 6b,d). We also note very similar features for the other seven top 10 extreme events for Orcadas station

during summer (Table 2 and Figures S4 and S5). It is worth noting that both the IVT vectors and 10 m wind anomalies tend to point southeastward.

Note that for both stations, the most extreme warm-temperature event during summer had a lower IVT value compared to the second warmest event (Figures 10 and 11). This indicates that the landfall IVT values may not be the best measure of the AR impact on temperature extremes. Instead, AR characteristics such as direction, length, duration and so forth, may also play an important role in shaping heat transport to the SOIs and influencing extreme temperatures. Additionally, localised föhn warming would also contribute to differences in the temperature extremes for these events (Table 2).

The circulation anomalies and the IVT morphology associated with the post-1979 top 10 winter warm-temperature extremes at both Signy and Orcadas stations are broadly similar to those for summer (cf. Figures S2–S5 and Figures S6–S9). However, compared to the summer events, it is evident that (a) the winter events involved more intense, deep polar cyclones or blocking highs with pressure anomalies in the region of ± 40 hPa or higher, and (b) the IVT magnitude near/to the west of the SOIs is generally smaller, likely because the amount of moisture transferred to the SOIs from the Pacific via the Drake Passage was lower in winter. The associated MSLP anomalies are also extreme, reaching either 99th or 1st percentiles at the corresponding locations (cf. Figures S7 & S9 versus Figure S1).

3.4 | Regional atmospheric model simulation

A detailed examination using high-resolution MetUM output enables us to explore how föhn warming could be responsible for the localised temperature extremes that characterise the SOIs. Comparison with results based on ERA5 can also give some quantification of the impact of orography, as ERA5 completely misrepresents this aspect, enabling us to disentangle the role of local (e.g., föhn warming) versus large-scale forcing (e.g., ARs and warm-air advection). In this section, we use the nested MetUM regional atmospheric model to simulate the second warmest of the top 10 warm events observed at Signy station during summer, which reached 17.4°C on 0000 UTC 13 January 1991 and involved föhn warming and an AR (Table 2 and Figure 10). Note that the warmest Signy event was already investigated by King *et al.* (2017).

The observations show that the peak temperature that occurred at 0000 UTC 13 January 1991 at Signy station was preceded by five consecutive warm events beginning from around 4 January and occurring roughly every

two days (Figure 12a). The observations also show that these episodes were accompanied by a rapid decrease in dew-point temperature (Figure 12a) and a sudden increase in wind speeds, which were generally northwesterly (Figure 12b); all these changes are characteristic of föhn events. In addition, the observations show that the MSLP time series exhibit a periodicity of around two days, with the peak in station temperatures coinciding with decreasing MSLP, that is, indicative of the approach of a series of depressions (Orr *et al.*, 2014).

These measurements/signatures of föhn at Signy station are captured reasonably well by the MetUM, with the model simulating a peak temperature of around 14°C at 2200 UTC 12 January 1991, that is, the simulated peak temperature is around 3°C lower and two hours earlier than the observed peak value of 17.4°C at 0000 UTC 13 January 1991 (Figure 12c,d). By contrast, although ERA5 captures the evolution of MSLP, it completely fails to capture the observed increases in temperature and wind speed and decreases in dew-point temperature (Figure 12e,f). In particular, the peak temperature at around 0000 UTC 13 January 1991 based on ERA5 is about 3°C , which is around 11°C lower than simulated by the MetUM and 14°C lower than observed. This suggests that up to 14°C of the warming can be attributed to föhn effects, with the rest of the warming attributed to large-scale advection of warm air from lower latitudes. One of the possible reasons for the discrepancy between the MetUM peak temperature and the observations is whether the vertical mixing in the boundary layer and the associated temperature structure is realistically simulated, for example in response to the downward penetration of föhn winds, which has been identified as a key model limitation (Elvidge *et al.*, 2016; Orr *et al.*, 2021).

Figure 13a shows the 10-m winds over the SOIs simulated by the MetUM at 0000 UTC 13 January 1991. At this time, the upstream simulated winds are northerly and decelerate down to around $5\text{ m}\cdot\text{s}^{-1}$ as they approach Coronation Island, indicative of low-level blocking of the flow by the steep orography (Orr *et al.*, 2004, 2008). This also gives rise to flow splitting around the SOIs (i.e., turning to both the right and left, and flowing around the island), and the formation of tip jets extending downstream and reaching $20\text{ m}\cdot\text{s}^{-1}$ when the wind reaches the end of the topographic barrier (Hunt *et al.*, 2004; Orr *et al.*, 2005, 2014; Hosking *et al.*, 2014). On the leeside of Coronation Island the 10-m winds strongly accelerate, reaching a peak of $25\text{--}30\text{ m}\cdot\text{s}^{-1}$ over its downslope region, as well as maintaining a wind speed of around $15\text{ m}\cdot\text{s}^{-1}$ in the downstream wake region (Risien and Chelton, 2008; Hosking *et al.*, 2014). Also apparent is a large increase in 1.5-m temperatures over southern (lee) slopes of Coronation Island compared to upstream values, with temperatures

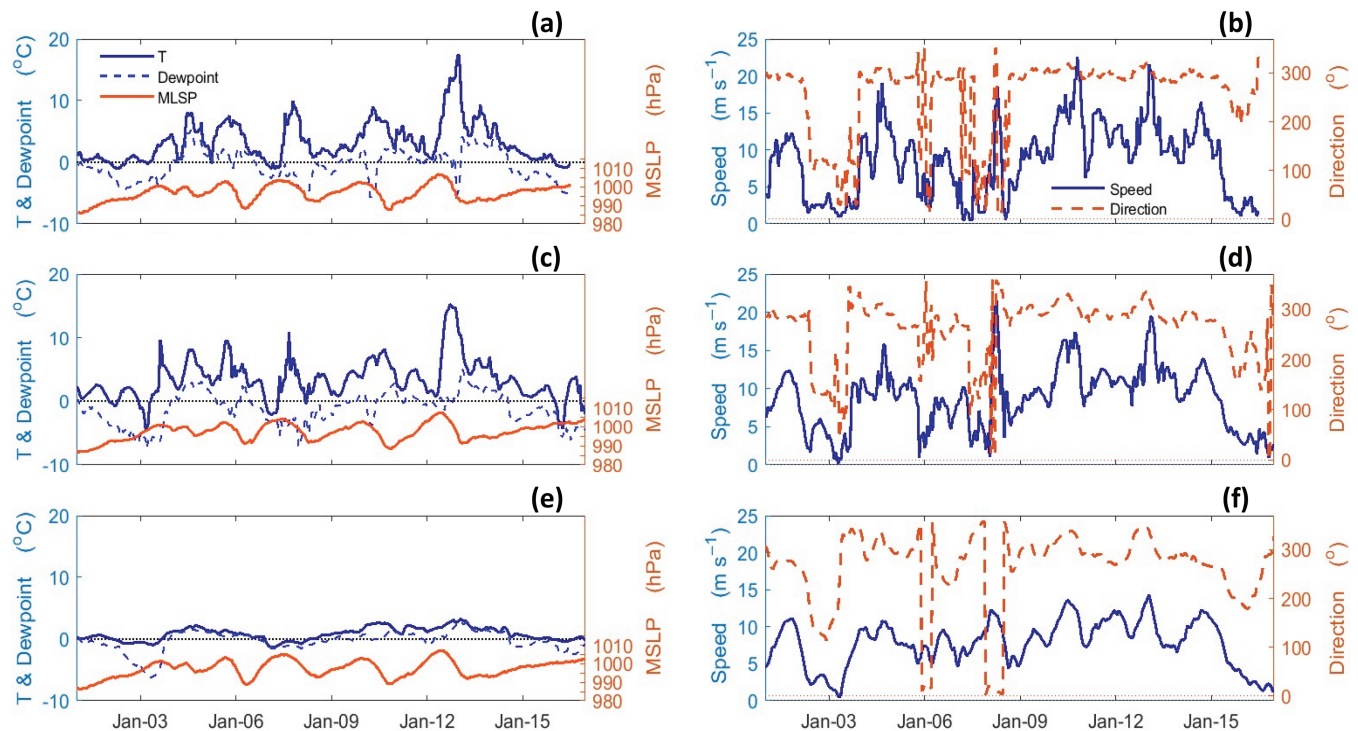


FIGURE 12 (a) Observed hourly time series of temperature ($^{\circ}\text{C}$; blue solid line), dew-point temperature ($^{\circ}\text{C}$; blue dashed line) and mean-sea-level pressure (hPa; orange line) observed at Signy station during the föhn wind case study from 1 to 17 January 1991. (b) As (a) but showing the observed time series of wind speed (m s^{-1} ; blue solid line) and wind direction ($^{\circ}$; dashed orange line). (c, d) As (a, b) but showing output from the MetUM simulation at 1-km grid spacing. (e, f) As (a, b) but showing output from ERA5 at the grid point where Signy station is located.

exceeding 10°C in many locations (Figure 13b). During this time the simulated temperature at Signy station is 9.4°C (cf. observed temperature of 17.4°C). Figure 13c shows that at 0000 UTC 13 January 1991 a substantial amount of rain also fell on the windward side of Coronation Island, with amounts exceeding 10 mm d^{-1} . The latent heat release due to the precipitation could therefore also contribute to the föhn warming on the leeward side (Elvidge and Renfrew, 2016). However, it is noticeable that the wind, precipitation, and temperature enhancement that occur on the upwind side of Coronation Island, north of Signy station, are not apparent near Laurie Island and therefore Orcadas station.

Figure 13d shows a cross-section of potential temperature and meridional wind speed along a north–south line across Coronation Island and Signy Island on 0000 UTC 13 January 1991. The potential temperature shows low-level blocking upstream from the surface to a height of around 400 m, with flow in this layer going around the obstacle rather than over it (Orr *et al.*, 2004, 2008). Flow above this level is able to pass over the barrier and generate mountain wave activity; especially evident is warm air descending from above the barrier down the leeside of Coronation Island to the surface (i.e., isentropic draw-down), as well as acceleration of the downslope winds. The

upstream flow at the height of the crest of the obstacle has a potential temperature of around 290 K (or 17°C), which is able to descend down much of the leeside of the barrier. However, at Signy station the potential temperature at the surface is around 282 K (9°C), which is consistent with Figure 13b.

4 | CONCLUSION AND DISCUSSION

Recent increases in the occurrence of warm-temperature extremes across the world have triggered extensive investigation into improving our understanding of their causes, including whether they are related to climate change (e.g., Coumou and Rahmstorf, 2012; Robinson, 2021). This study contributes towards the effort by identifying atmospheric circulation patterns and long-term trends that are associated with extreme warm events at Signy and Orcadas stations in the SOIs, defined as events with temperatures exceeding the 95th percentile of the temperature distribution. For both stations, the temperature threshold that characterises the 95th percentile of station-based synoptic observations exceeds the melting point of ice/snow for summer and winter (Figure 2, Table 1). Moreover, we find

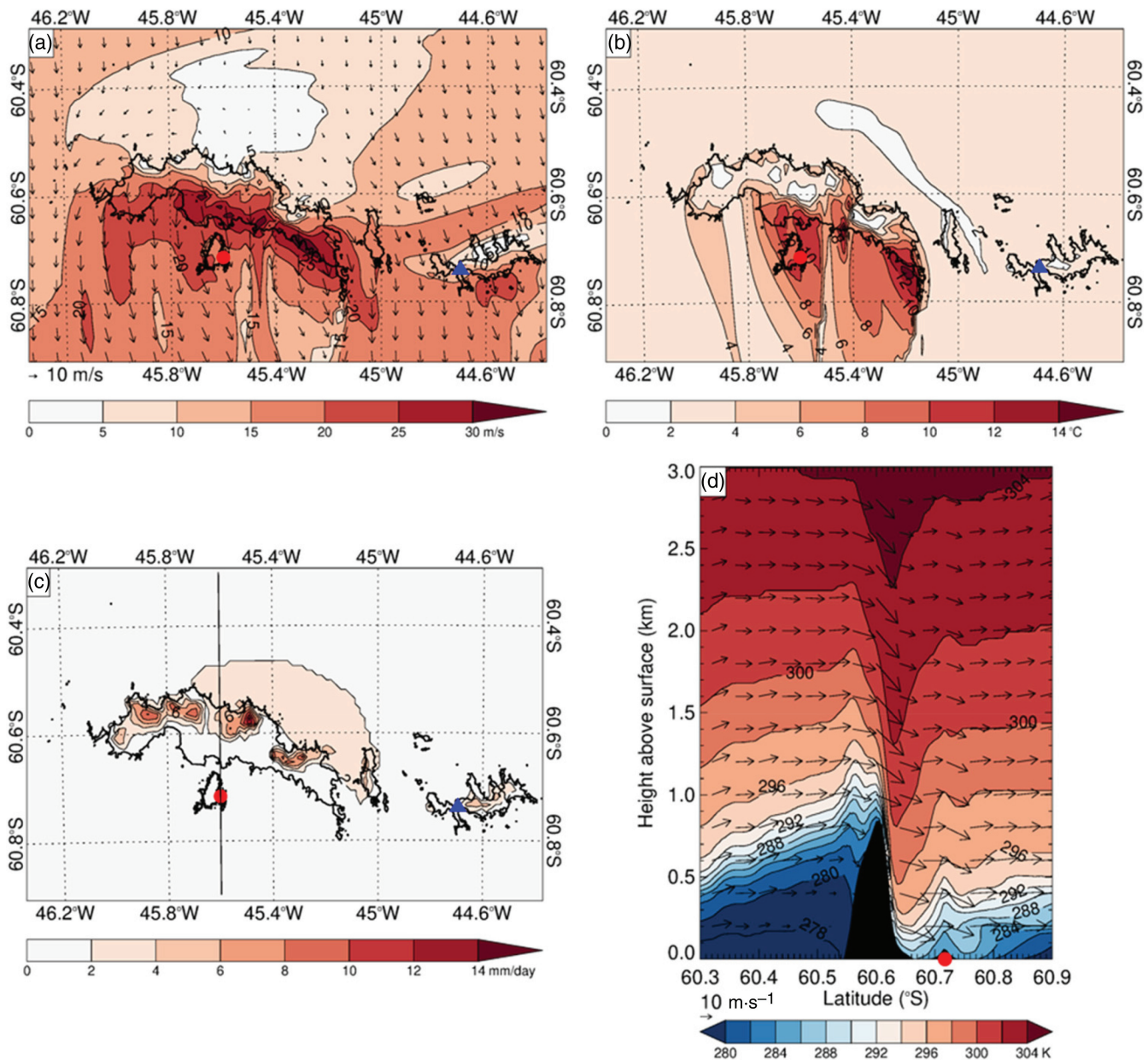


FIGURE 13 Output from the MetUM simulation at 1-km grid spacing during the föhn wind case study on 0000 UTC 13 January 1991 over the SOIs of (a) 10-m wind field ($\text{m}\cdot\text{s}^{-1}$; arrows) and magnitude ($\text{m}\cdot\text{s}^{-1}$; contours), (b) temperature at 1.5 m ($^{\circ}\text{C}$), (c) rain ($\text{mm}\cdot\text{d}^{-1}$; averaged over three-hour period), and (d) potential temperature (K; shading) and meridional wind ($\text{m}\cdot\text{s}^{-1}$; arrows) along a north-south vertical cross section through the location of Signy station at 45.6°W . The transect used for the cross-section is shown by the solid black line in panel (c). In all panels the locations of Signy and Orcadas stations are marked by the red dot and blue triangle respectively.

positive trends in the number of events each year that exceed this threshold at both stations (Figure 4). Such an increase in extreme warm-event occurrence may result in increased ice/snow melting in the SOIs.

Recent studies indicate that the combined effect of ARs and föhn warming contribute to the melting of the cryosphere in the eastern and western parts of the Antarctic Peninsula (e.g., Wille *et al.*, 2022). However, limited research has been conducted to assess the impact of

these mechanisms on Antarctic maritime islands and the surface mass balance in the northern Antarctic Peninsula (Bozkurt *et al.*, 2018). The results presented in this study provide strong evidence that the warm extremes over the SOIs involve a combination of ARs and leeside föhn warming, particularly by examining the top 10 warmest events for both summer and winter at Signy and Orcadas stations (Tables 2 and 3), and thus a potential role in melting events and glacier retreat in the region.

The ARs are associated with anomalous strong northerly, northwesterly, or westerly winds, associated with a dipole in MSLP near the SOIs (Figure 6), which advect relatively warm, moist air masses towards the SOIs (Figure 8). However, the localised föhn warming is likely responsible for the differences in warm extremes between the two stations, and more generally for the highly variable spatial patterns of extremes across the SOIs due to their complex orography. In particular, Signy extreme-temperature thresholds are about 1°C warmer than those for Orcadas on average (Table 1), which may be explained by localised föhn effects in relation to Coronation Island. Additionally, warm events at Signy are warmer (by an average of around 3°C) than the corresponding concurrent temperatures at Orcadas (Figure 5). At Signy, föhn warming is associated with the interaction of northerly winds with Coronation Island, while at Orcadas the föhn warming is associated with northwesterlies/westerlies that interact with Coronation Island. These fine-scale effects are not captured by ERA5. The contrasting mechanisms over such relatively short distances between Signy and Orcadas (51 km) highlights the importance of a detailed approach to understanding extremes over regions with complex orography.

Adiabatic descent of upper-level warm air plays an important role as a key mechanism of föhn dynamics in the SOIs. Using the high temperature event that occurred on 13 January 1991 at Signy as a case study, we further demonstrated that the adiabatic descent of upper-level warm air on the leeside of Coronation Island plays the most important role (Figure 13). The event was associated with the occurrence of four or five individual extreme warm events along with the southward advection of an exceptionally warm, moist air mass from the South Atlantic along the eastern side of the Andes (Figure 12). This was followed by a final föhn warming at Signy station due to the strong northerlies that flowed over Coronation Island, causing near-surface temperature at Signy to rise suddenly up to 17°C (Figures 12 and 13).

Our result that the occurrence of station warm extremes increases with time is consistent with the finding of Turner *et al.* (2021). Such increases in annual percentage of station warm extremes occur alongside positive trends in the occurrence of the pressure difference associated with the dipole pattern (Figure 7). Such increases in both the warm extreme occurrences at the stations and their regional drivers are possibly linked to a latitudinal shift of the storm tracks in association with the El Niño-Southern Oscillation (ENSO) (Turner, 2004; Turner *et al.*, 2016). Machado *et al.* (2021) found that there has been a latitudinal migration of the storm tracks in summer in association with ENSO. The position of the storm tracks is also strongly influenced by the Southern

Annular Mode (SAM; Marshall, 2003, 2007). The period with a positive trend in the occurrence of extreme warm events in the SOIs coincides with a period of positive summertime SAM trends (Marshall, 2003, 2007). This would result in a stronger, more poleward-shifted storm track, which in turn would bring in increased warm, humid air from lower latitudes and thus increase temperature in the SOIs. The positive trend in extreme warm events in the SOIs may also be linked to the enhancement of zonal wave-3 pattern and associated blocking anomalies (Goyal *et al.*, 2022; Bozkurt *et al.*, 2022).

Signy Island is unique as it supports a terrestrial ecosystem that is one of the richest and most biodiverse anywhere in the maritime Antarctic (Smith, 1990). Indirect studies based on biological proxies, for example, vegetation surveys or carbon isotopes, indicate that Signy Island has experienced the most rapid atmospheric warming in the Antarctic region (e.g., Cannone *et al.*, 2017; Convey, 2017; Convey and Peck, 2019). Based on continuous meteorological records at Signy, for the first time, we have demonstrated that the warm trends observed by these biological proxies were mostly associated with the increased recurrence of large-scale circulation anomalies in the region and their interaction with local topography. Whilst this study is focusing on the SOIs, the findings will inform our understanding of extremes on other sub-Antarctic islands, as well as over the complex coastline of Antarctica itself.

AUTHOR CONTRIBUTIONS

Hua Lu: Conceptualization; data curation; formal analysis; funding acquisition; investigation; methodology; project administration; software; validation; writing – original draft; writing – review and editing. **Andrew Orr:** Conceptualization; formal analysis; investigation; methodology; software; validation; writing – original draft; writing – review and editing. **John King:** Conceptualization; formal analysis; investigation; methodology; validation; writing – review and editing. **Tony Phillips:** Data curation; formal analysis; software; validation; visualization. **Ella Gilbert:** Software; writing – review and editing. **Steve Colwell:** Data curation; writing – review and editing. **Thomas J. Bracegirdle:** Writing – review and editing.

ACKNOWLEDGEMENTS

This work is supported by core funding from the Natural Environment Research Council (NERC) to the Atmosphere, Ice and Climate Programme of British Antarctic Survey (BAS). Hua Lu, Andrew Orr, and Thomas J. Bracegirdle have received support from the NERC National Capability International grant SURface FluxEs In Antarctica (NE/X009319/1). Andrew Orr and Ella Gilbert are supported by the European Union's Horizon 2020

research and innovation framework programme under grant agreement no. 101003590 (PolarRES). We are grateful for the expert comments by two anonymous referees that improved the original manuscript. Laura Gerrish is thanked for helping plotting Figure 1. We also thank Emilia Dobb, Jonathan Xue, Sabina Kucieba, Guy Phillips, and the BAS archive team for their efforts in digitizing and quality control of the Signy records, and funding from NERC Diversity, Equity and Inclusion (DEI) Engagement Programme. Kyle Clem and Peter Convey are thanked for helpful discussions in examining the trends and the impact on the ecosystem.

FUNDING INFORMATION

This work is supported by core funding from the Natural Environment Research Council (NERC) to the Atmosphere, Ice and Climate Programme of British Antarctic Survey (BAS). Hua Lu, Andrew Orr, and Thomas J. Bracegirdle have received support from the NERC National Capability International grant SURface FluxEs In AnTartica (NE/X009319/1). Andrew Orr and Ella Gilbert are supported by the European Union's Horizon 2020 research and innovation framework programme under grant agreement no. 101003590 (PolarRES).

DATA AVAILABILITY STATEMENT

ERA5 data were accessed from the Climate Data Store (CDS) provided by the Copernicus program. The Orcadas station data are available from the READER website https://legacy.bas.ac.uk/met/READER/ANTARCTIC_METEOROLOGICAL_DATA/SURFACE/Orcadas_surface.dat. The Signy station data (Colwell and Lu, 2023) are available from the UK Polar Data Centre (PDC) website: <https://doi.org/10.5285/d74b142c-7981-4a6a-9321-cf904a5668e6>. The MetUM model output (Orr and Phillips, 2023) is available from the UK PDC (UK Polar Data Centre) website: <https://doi.org/10.5285/0b011472-c766-4190-8718-8cf4be95daa6>. The AR database (<http://10.099.2/S6/YO15ON>) was provided by Bin Guan via the Global Atmospheric Rivers Dataverse (<https://dataverse.ucla.edu/dataverse/ar>) to extract the AR shapes and to estimate the AR landfall statistics.

ORCID

Hua Lu  <https://orcid.org/0000-0001-9485-5082>

Andrew Orr  <https://orcid.org/0000-0001-5111-8402>

REFERENCES

- Alexander, L.V. and Arblaster, J.M. (2009) Assessing trends in observed and modelled climate extremes over Australia in relation to future projections. *International Journal of Climatology*, 29, 417–435. <https://doi.org/10.1002/joc.1730>.
- Alexander, M.J., Eckermann, S.D., Broutman, D. and Ma, J. (2009) Momentum flux estimates for South Georgia Island mountain waves in the stratosphere observed via satellite. *Geophysical Research Letters*, 36, L12816. <https://doi.org/10.1029/2009GL038587>.
- Alves, J.M.R., Tomé, R., Caldeira, R.M.A. and Miranda, P.M.A. (2021) Asymmetric Ocean response to atmospheric forcing in an Island wake: a 35-year high-resolution study. *Frontiers in Marine Science*, 8, 624392. <https://doi.org/10.3389/fmars.2021.624392>.
- Bannister, D. and King, J.C. (2020) The characteristics and temporal variability of föhn winds at King Edward point, South Georgia. *International Journal of Climatology*, 2020(40), 2778–2794. <https://doi.org/10.1002/joc.6366>.
- Bozkurt, D., Marin, J. and Barrett, B. (2022) Temperature and moisture transport during atmospheric blocking patterns around the Antarctic peninsula. *Weather and Climate Extremes*, 38, 100506. <https://doi.org/10.1016/j.wace.2022.100506>.
- Bozkurt, D., Rondanelli, R., Marin, J.C. and Garreaud, R. (2018) Foehn event triggered by an atmospheric river underlies record-setting temperature along continental Antarctica. *Journal of Geophysical Research – Atmospheres*, 123, 3871–3892. <https://doi.org/10.1002/2017JD027796>.
- Bush, M., Allen, T., Bain, C., Boutle, I., Edwards, J., Finnenkoetter, A., Franklin, C., Hanley, K., Lean, H., Lock, A., Manners, J., Mittermaier, M., Morcrette, C., North, R., Petch, J., Short, C., Vosper, S., Walters, D., Webster, S., Weeks, M., Wilkinson, J., Wood, N. and Zerroukat, M. (2020) The first Met Office Unified Model–JULES regional atmosphere and land configuration, RAL1. *Geoscientific Model Development*, 13, 1999–2029. <https://doi.org/10.5194/gmd-13-1999-2020>.
- Calosi, P., Bilton, B.T. and Spicer, J.I. (2008) Thermal tolerance, acclimatory capacity and vulnerability to global climate change. *Biology Letters*, 4, 99–102. <https://doi.org/10.1098/rsbl.2007.0408>.
- Cannone, N., Fratte, M.D., Convey, P., Worland, M.R. and Guglielmin, M. (2017) Ecology of moss banks on Signy Island (maritime Antarctic). *Botanical Journal of the Linnean Society*, 184, 518–533. <https://doi.org/10.1093/botlinnean/box040>.
- Colesie, C., Walshaw, C.V., Sancho, L.G., Davey, M.P. and Gray, A. (2023) Antarctica's vegetation in a changing climate. *WIREs Climate Change*, 14(1), e810. <https://doi.org/10.1002/wcc.810>.
- Colwell, S., and Lu, H. (2023) Continuous subdaily meteorological records at Signy Station, the South Orkney Islands 1947 - 1994 (Version 1.0) [Data set]. NERC EDS UK Polar Data Centre. <https://doi.org/10.5285/d74b142c-7981-4a6a-9321-cf904a5668e6>.
- Convey, P. (2017) Antarctic ecosystems. In: *Reference Module in Life Sciences*. Elsevier, ISBN 9780128096338. <https://doi.org/10.1016/B978-0-12-809633-8.02182-8>.
- Convey, P. and Peck, L.S. (2019) Antarctic environmental change and biological responses. *Science Advances*, 11, eaaz0888.
- Coumou, D. and Rahmstorf, S. (2012) A decade of weather extremes. *Nature Climate Change*, 2, 491–496. <https://doi.org/10.1038/nclimate1452>.
- Elvidge, A.D. and Renfrew, I.A. (2016) The causes of föhn warming in the lee of mountains. *Bulletin of the American Meteorological Society*, 97, 455–466. <https://doi.org/10.1175/BAMS-D-14-00194.1>.
- Elvidge, A.D., Renfrew, I.A., King, J.C., Orr, A. and Lachlan-Cope, T.A. (2016) Föhn warming distributions in nonlinear and linear flow regimes: a focus on the Antarctic peninsula. *Quarterly Journal of the Royal Meteorological Society*, 142, 618–631.

- Elvidge, A.D., Renfrew, I.A., King, J.C., Orr, A., Lachlan-Cope, T.A., Weeks, M. and Gray, S.L. (2015) Föhn jets over the Larsen C ice shelf, Antarctica. *Quarterly Journal of the Royal Meteorological Society*, 141, 698–713. <https://doi.org/10.1002/qj.2382>.
- Gilbert, E., Orr, A., King, J.C., Renfrew, I.A. and Lachlan-Cope, T.A. (2022) A 20-year study of melt processes over Larsen C ice shelf using a high-resolution regional atmospheric model: 1. Model configuration and validation. *Journal of Geophysical Research – Atmospheres*, 127, e2021JD034766. <https://doi.org/10.1029/2021JD034766>.
- Gilbert, E., Orr, A., King, J.C., Renfrew, I.A., Lachlan-Cope, T.A., Field, P. and Boutle, I. (2020) Summertime cloud phase strongly influences surface melting on the Larsen C ice shelf Antarctica. *Quarterly Journal of the Royal Meteorological Society*, 146, 1575–1589. <https://doi.org/10.1002/qj.3753>.
- Goyal, R., Jucker, M., Gupta, A.S. and England, M.H. (2022) A new zonal Wave-3 index for the southern hemisphere. *Journal of Climate*, 35(15), 5137–5149. <https://doi.org/10.1175/JCLI-D-21-0927.1>.
- Guan, B. and Waliser, D.E. (2019) Tracking atmospheric rivers globally: spatial distributions and temporal evolution of life cycle characteristics. *Journal of Geophysical Research – Atmospheres*, 124, 12523–12552. <https://doi.org/10.1029/2019JD031205>.
- Hersbach, H., Bell, B., Berrisford, P., Hirahara, S., Horányi, A., Muñoz-Sabater, J., Nicolas, J., Peubey, C., Radu, R., Schepers, D., Simmons, A., Soci, C., Abdalla, S., Abellan, X., Balsamo, G., Bechtold, P., Biavati, G., Bidlot, J., Bonavita, M., de Chiara, G., Dahlgren, P., Dee, D., Diamantakis, M., Dragani, R., Flemming, J., Forbes, R., Fuentes, M., Geer, A., Haimberger, L., Healy, S., Hogan, R.J., Hólm, E., Janisková, M., Keeley, S., Laloyaux, P., Lopez, P., Lupu, C., Radnoti, G., de Rosnay, P., Rozum, I., Vamborg, F., Villaume, S. and Thépaut, J.N. (2020) The ERA5 global reanalysis. *Quarterly Journal of the Royal Meteorological Society*, 146, 1999–2049. <https://doi.org/10.1002/qj.3803>.
- Hosking, J.S., Bannister, D., Orr, A., King, J., Young, E. and Phillips, T. (2014) Orographic forcing of surface winds over the shelf waters adjacent to South Georgia. *Atmospheric Science Letters*, 16, 50–55. <https://doi.org/10.1002/asl2.519>.
- Hoskins, B.J. and Hodges, K.I. (2005) A new perspective on southern hemisphere storm tracks. *Journal of Climate*, 18, 4108–4129. <https://doi.org/10.1175/JCLI3570.1>.
- Howat, I., et al. (2022) The Reference Elevation Model of Antarctica – Mosaics, Version 2. <https://doi.org/10.7910/DVN/EBW8UC>, Harvard Dataverse [accessed January 2023].
- Hunt, J.C.R., Orr, A., Rottman, J.W. and Capon, R. (2004) Coriolis effects in mesoscale flows with sharp changes in surface conditions. *Quarterly Journal of the Royal Meteorological Society*, 130, 2703–2731. <https://doi.org/10.1256/qj.04.14>.
- King, J.C., Bannister, D., Hosking, J.S. and Colwell, S.R. (2017) Causes of the Antarctic region record high temperature at Signy Island, 30th January 1982. *Atmospheric Science Letters*, 18, 491–496. <https://doi.org/10.1002/asl.793>.
- Liu, H., Jezek, K., Li, B. and Zhao, Z. (2015) *Radarsat Antarctic Mapping Project Digital Elevation Model Version 9*. Boulder, CO: NASA National Snow and Ice Data Center Distributed Active Archive Center. <https://doi.org/10.5067/8JKNEW6BFRVD>.
- Machado, J.P., Justino, F. and Souza, C.D. (2021) Influence of El Niño-southern oscillation on baroclinic instability and storm tracks in the southern hemisphere. *International Journal of Climatology*, 41(Suppl. 1), E93–E109. <https://doi.org/10.1002/joc.6651>.
- MacLennan, M.L., Lenaerts, J.T.M., Shields, C. and Wille, J.D. (2022) Contribution of atmospheric rivers to Antarctic precipitation. *Geophysical Research Letters*, 49, e2022GL100585. <https://doi.org/10.1029/2022GL100585>.
- Marshall, G.J. (2003) Trends in the southern annular mode from observations and reanalyses. *Journal of Climate*, 16, 4134–4143. [https://doi.org/10.1175/1520-0442\(2003\)016%3c4134:TITSAM%3e2.0.CO;2](https://doi.org/10.1175/1520-0442(2003)016%3c4134:TITSAM%3e2.0.CO;2).
- Marshall, G.J. (2007) Half-century seasonal relationships between the southern annular mode and Antarctic temperatures. *International Journal of Climatology*, 27, 373–383. <https://doi.org/10.1002/joc.1407>.
- Meredith, M.P., Meijers, A.S., Naveira Garabato, A.C., Brown, P.J., Venables, H.J., Abrahamsen, E.P., Jullion, L. and Messias, M.-J. (2015) Circulation, retention, and mixing of waters within the Weddell-scotia confluence, Southern Ocean: the role of stratified Taylor columns. *Journal of Geophysical Research, Oceans*, 120, 547–562. <https://doi.org/10.1002/2014JC010462>.
- Montini, T.L., Jones, C. and Carvalho, L.M.V. (2019) The south American low-level jet: a new climatology, variability, and changes. *Journal of Geophysical Research – Atmospheres*, 124, 1200–1218. <https://doi.org/10.1029/2018JD029634>.
- Orr, A., Cresswell, D., Marshall, G.J., Hunt, J.C.R., Sommeria, J. and Wang, C.G. (2004) A ‘low-level’ explanation for the recent large warming trend over the western Antarctic peninsula involving blocked winds and changes in zonal circulation. *Geophysical Research Letters*, 31, L06204. <https://doi.org/10.1029/2003GL019160>.
- Orr, A., Deb, P., Clem, K., Gilbert, E., Bromwich, D., Boberg, F., Colwell, S., Hansen, N., Lazzara, M., Mooney, P., Mottram, R., Niwano, N., Phillips, T., Pishniak, D., Riejmer, C., van de Berg, W.J., Webster, S. and Zou, X. (2023) Characteristics of surface “melt potential” over Antarctic ice shelves based on regional atmospheric model simulations of summer air temperature extremes from 1979/80 to 2018/19. *Journal of Climate*, 36, 3357–3383. <https://doi.org/10.1175/JCLI-D-22-0386.1>.
- Orr, A., Hunt, J., Capon, R., Sommeria, J., Cresswell, D. and Owinoh, A. (2005) Coriolis effects on wind jets and cloudiness along coasts. *Weather*, 60, 291–299. <https://doi.org/10.1256/wea.219.04>.
- Orr, A., Kirchgassner, A., King, J., Phillips, T., Gilbert, E., Elvidge, A., Weeks, M., Gadian, A., Kuipers Munneke, P., van den Broeke, M., Webster, S. and McGrath, D. (2021) Comparison of kilometre and sub-kilometre scale simulations of a foehn wind event over the Larsen C ice shelf using the met Office unified model (MetUM). *Quarterly Journal of the Royal Meteorological Society*, 147, 3472–3492. <https://doi.org/10.1002/qj.4138>.
- Orr, A., Marshall, G.J., Hunt, J.C.R., Sommeria, J., Wang, C.G., van Lipzig, N.P.M., Cresswell, D. and King, J.C. (2008) Characteristics of airflow over the Antarctic peninsula and its response to recent strengthening of westerly circumpolar winds. *Journal of the Atmospheric Sciences*, 65, 1396–1413. <https://doi.org/10.1175/2007JAS2498.1>.
- Orr, A., and Phillips, T. (2023) MetUM high-resolution simulations of extreme warm temperature events over South Orkney Islands from 1 to 17 January 1991 (Version 1.0) [Data set]. NERC EDS UK Polar Data Centre. <https://doi.org/10.5285/0b011472-c766-4190-8718-8cf4be95daa6>.

- Orr, A., Phillips, T., Webster, S., Elvidge, A., Weeks, M., Hosking, S. and Turner, J. (2014) Met office unified model high-resolution simulations of a strong wind event in Antarctica. *Quarterly Journal of the Royal Meteorological Society*, 140, 2287–2297. <https://doi.org/10.1002/qj.2296>.
- Peterson, R.G. and Stramma, L. (1991) Upper-level circulation in the South Atlantic Ocean. *Progress in Oceanography*, 26, 1–73. [https://doi.org/10.1016/0079-6611\(91\)90006-8](https://doi.org/10.1016/0079-6611(91)90006-8).
- Ramos, A.M., Blamey, R.C., Algarra, I., Nieto, R., Gimeno, L., Tomé, R., Reason, C.J.C. and Trigo, R.M. (2019) From Amazonia to southern Africa: atmospheric moisture transport through low-level jets and atmospheric rivers. *Annals of the New York Academy of Sciences*, 1436, 217–230. <https://doi.org/10.1111/nyas.139602019>.
- Risien, C.M. and Chelton, D.B. (2008) A global climatology of surface wind and wind stress fields from eight years of QuikSCAT scatterometer data. *Journal of Physical Oceanography*, 38, 2379–2413. <https://doi.org/10.1175/2008JPO3881.1>.
- Robinson, W.A. (2021) Climate change and extreme weather: a review focusing on the continental United States. *Journal of the Air & Waste Management Association*, 71(10), 1186–1209. <https://doi.org/10.1080/10962247.2021.1942319>.
- Sanchez, N., Reiss, C.S., Holm-Hansen, O., Hewes, C.D., Bizsel, K.C. and Ardelan, M.V. (2019) Weddell-Scotia confluence effect on the iron distribution in waters surrounding the south Shetland (Antarctic peninsula) and South Orkney (Scotia Sea) islands during the austral summer in 2007 and 2008. *Frontiers in Marine Science*, 6, 00771. <https://doi.org/10.3389/fmars.2019.00771>.
- Simmons, A.J. and Hollingsworth, A. (2002) Some aspects of the improvement in skill of numerical weather prediction. *Quarterly Journal of the Royal Meteorological Society*, 128(580), 647–677.
- Smith, R.I.L. (1990) Signy Island as a paradigm of biological and environmental change in Antarctic terrestrial ecosystems. In: Kerry, K.R. and Hempel, G. (Eds.) *Antarctic Ecosystems*. Berlin, Heidelberg: Springer. https://doi.org/10.1007/978-3-642-84074-6_4.
- Trenberth, K.E. (1991) Storm tracks in the southern hemisphere. *Journal of the Atmospheric Sciences*, 48, 2159–2178. [https://doi.org/10.1175/1520-0469\(1991\)048<2159:STITSH>2.0.CO;2](https://doi.org/10.1175/1520-0469(1991)048<2159:STITSH>2.0.CO;2).
- Turner, J. (2004) The El Niño-southern oscillation and Antarctica. *International Journal of Climatology*, 24(1), 1–31. <https://doi.org/10.1002/joc.965>.
- Turner, J., Colwell, S.R., Marshall, G.J., Lachlan-Cope, T.A., Carleton, A.M., Jones, P.D., Lagun, V., Reid, P.A. and Iagovkina, S. (2004) The SCAR READER project: toward a high-quality database of mean Antarctic meteorological observations. *Journal of Climate*, 17, 2890–2898. [https://doi.org/10.1175/1520-0442\(2004\)017<2890:TSRPTA>2.0.CO;2](https://doi.org/10.1175/1520-0442(2004)017<2890:TSRPTA>2.0.CO;2).
- Turner, J., Lu, H., King, J.C., Marshall, G.J., Phillips, T., Bannister, D. and Colwell, S. (2021) Extreme temperatures in the Antarctic. *Journal of Climate*, 34, 2653–2668. <https://doi.org/10.1175/JCLI-D-20-0538.1>.
- Turner, J., Lu, H., White, I., King, J.C., Phillips, T., Hosking, J.S., Bracegirdle, T.J., Marshall, G.J., Mulvaney, R. and Deb, P. (2016) Absence of 21st century warming on Antarctic peninsula consistent with natural variability. *Nature*, 535, 411–415. <https://doi.org/10.1038/nature18645>.
- Wille, J.D., Favier, V., Dufour, A., Gorodetskaya, I.V., Turner, J., Agosta, C. and Codron, F. (2019) West Antarctic surface melt triggered by atmospheric rivers. *Nature Geoscience*, 12, 911–916. <https://doi.org/10.1038/s41561-019-0460-1>.
- Wille, J.D., Favier, V., Jourdain, N.C., Kittel, C., Turton, J.V., Agosta, C., Gorodetskaya, I.V., Picard, G., Codron, F., Santos, C.L.D., Amory, C., Fettweis, X., Blanchet, J., Jomelli, V. and Berchet, A. (2022) Intense atmospheric rivers can weaken ice shelf stability at the Antarctic peninsula. *Communications Earth & Environment*, 3, 90. <https://doi.org/10.1038/s43247-022-00422-9>.
- Wood, N., Staniforth, A., White, A., Allen, T., Diamantakis, M., Gross, M., Melvin, T., Smith, C., Vosper, S., Zerroukat, M. and Thuburn, J. (2014) An inherently mass-conserving semi-implicit semi-Lagrangian discretization of the deep-atmosphere global non-hydrostatic equations. *Quarterly Journal of the Royal Meteorological Society*, 140, 1505–1520. <https://doi.org/10.1002/qj.2235>.
- Yuan, X. (2004) High-wind-speed evaluation in the Southern Ocean. *Journal of Geophysical Research*, 109, D13101. <https://doi.org/10.1029/2003JD004179>.
- Zhang, Z., Ralph, F.M. and Zheng, M. (2019) The relationship between extratropical cyclone strength and atmospheric river intensity and position. *Geophysical Research Letters*, 46, 1814–1823. <https://doi.org/10.1029/2018GL079071>.

SUPPORTING INFORMATION

Additional supporting information can be found online in the Supporting Information section at the end of this article.

How to cite this article: Lu, H., Orr, A., King, J., Phillips, T., Gilbert, E., Colwell, S. *et al.* (2023) Extreme warm events in the South Orkney Islands, Southern Ocean: Compounding influence of atmospheric rivers and föhn conditions. *Quarterly Journal of the Royal Meteorological Society*, 1–24. Available from: <https://doi.org/10.1002/qj.4578>